Systematic analysis uncovers SYK dependency in NF1^{LoF} melanoma cells

Cara Abecunas [1,2], Christopher Whitehead [3], Elizabeth Ziemke [3], Douglas G. Baumann [1,7], Christy Frankowski-McGregor [3], Judith Sebolt-Leopold [3,4,5], and Mohammad Fallahi-Sichani [1,6]

[1] Department of Biomedical Engineering, University of Virginia, Charlottesville, VA 22908

[2] Department of Biomedical Engineering, University of Michigan, Ann Arbor, MI 48109

[3] Department of Radiology, University of Michigan Medical School, Ann Arbor, MI 48109

[4] Department of Pharmacology, University of Michigan Medical School, Ann Arbor, MI 48109

[5] Rogel Cancer Center, University of Michigan, Ann Arbor, MI 48109

[6] UVA Comprehensive Cancer Center, University of Virginia, Charlottesville, VA 22908

[7] Present address: Dewpoint Therapeutics, 451 D Street, Suite 104, Boston, MA 02210

Address correspondence to:

Mohammad Fallahi-Sichani

Address: 415 Lane Rd, Building MR5, Room 2215, Charlottesville, VA 22903

ORCID ID: 0000-0003-0917-3525

Tel/Fax: (434) 924-9950

Email: fallahi@virginia.edu

Abstract

The loss of function (LoF) of NF1 is the third most frequent mutation that drives hyperactivated RAS and tumor growth in >10% of melanomas. $NF1^{LoF}$ melanoma cells, however, do not show consistent sensitivity to individual MEK, ERK, or PI3K/mTOR inhibitors. Here, we perform a targeted kinase inhibitor screen and identify a tool compound, named MTX-216, to be highly effective in blocking $NF1^{LoF}$ melanoma cells. Single-cell analysis links drug-induced cytotoxicity to effective co-suppression of proliferation marker Ki-67 and the ribosomal S6 phosphorylation, an integrator of multiple RAS-mediated signaling pathways. Using a combination of kinome selectivity assay, transcriptomic analysis, and genetic experiments, we find the anti-tumor efficacy of MTX-216 to be dependent on its ability to inhibit not only PI3K (its nominal target) but also SYK, and suppression of a group of genes that regulate mitochondrial electron transport chain and whose expression is associated with poor survival in $NF1^{LoF}$ melanoma patients. Furthermore, combinations of inhibitors targeting either MEK or PI3K/mTOR with an independent SYK kinase inhibitor or SYK knockdown show favorable effects. These studies provide a path to exploit SYK dependency to selectively block $NF1^{LoF}$ melanoma cells.

Introduction

Oncogenic activation of the RAS/MAPK signaling pathway occurs across >90% of melanomas [1]. However, only those tumors that are driven by $BRAF^{V600E/K/D}$ mutations have shown consistent clinical responses to standard-of-care MAPK-targeted therapies [2]. Neurofibromin 1 (NF1) is a tumor suppressor gene encoding a RAS GTPase-activating protein, whose loss of function (LoF) is the third most frequent mutation present in approximately 13% of melanomas [1,3–5]. $NF1^{LoF}$ mutations abrogate negative feedback on RAS, thereby causing hyperactivation of the downstream MAPK and PI3K/mTOR signaling pathways [6,7]. NF1 mutations, however, do not always predict sensitivity to either MEK/ERK

kinase inhibitors or PI3K/mTOR inhibitors and most $NF1^{LoF}$ melanomas show only partial responses to these therapies [8–10]. There is a need for the identification of more effective strategies to block tumor growth in $NF1^{LoF}$ melanomas, for which efficient targeted therapies are currently unavailable.

Multiple strategies have been tested to enhance treatment efficacy in $NF1^{LoF}$ melanomas. The most commonly explored approaches have been focused on testing combinations of small molecules (e.g., MEK/ERK inhibitors and PI3K/mTOR inhibitors) that target parallel pathways downstream of RAS signaling, in order to prevent the bypass mechanisms of drug resistance [11]. These combinations, however, have not yet produced sufficient benefit to warrant their use in clinical studies. Targeting RAS regulators that function downstream of receptor tyrosine kinases (RTKs), such as EGFR, has been proposed as another strategy based on the evidence that $NF1^{LoF}$ cells require upstream RTK signals to drive aberrant cell growth [12]. SHP2 inhibitors, for example, decouple the RAS/MAPK pathway from external growth signals (e.g., EGF/EGFR signaling) and thereby reduce tumor growth in $NF1^{LoF}$ melanoma cells [13]. An alternative strategy would be to evaluate the effectiveness of multi-targeted inhibitors that block key signaling molecules upstream and downstream of RAS [14,15]. A possible advantage of this approach may be a further increase in treatment efficacy that results from co-targeting the pathways on which $NF1^{LoF}$ cell growth and survival are dependent as well as adaptive pathways that diminish the efficacy of individual MEK/ERK or PI3K/mTOR inhibitors.

In this paper, we perform a targeted compound screen to search for actionable kinases upstream, parallel to, or downstream of MAPK and PI3K/mTOR pathways, whose inhibition individually or in combination with one another lead to lethality of $NF1^{LoF}$ melanoma cells. We identify MTX-216, a dual ATP-competitive inhibitor of PI3K isoforms and EGFR, to kill $NF1^{LoF}$ melanoma cells in a dose-dependent manner and block $NF1^{LoF}$ melanoma tumor growth *in vivo*. MTX-216 has only minimal effect on non-transformed primary melanocytes or $BRAF^{V600E}$-mutated cells but induces apoptosis in

NF1^{LoF} melanoma cells with a greater efficacy in comparison with equivalent doses of other tested small molecules, including inhibitors of MEK, ERK, pan-PI3K, mTORC1/2, EGFR and CDK4/6. Single-cell analysis reveals a substantial correlation between drug-induced cytotoxicity and effective co-suppression of Ki-67 (a proliferation marker) and the ribosomal S6 phosphorylation (an integrator of multiple RAS-mediated signaling pathways) in NF1^{LoF} melanoma cells. These effects, however, are not explained merely by the nominal targets of MTX-216. Interestingly, MTX-211, a structural analogue of MTX-216 with comparable potency against PI3K isoforms and EGFR, does not elicit an efficacious response in NF1^{LoF} melanoma cells. Kinome selectivity analysis integrated with differential gene expression and pathway enrichment analysis lead us to identify SYK, a non-receptor tyrosine kinase and a mediator of the oxidative mitochondrial respiratory chain [16], as an additional target of MTX-216 that is required for NF1^{LoF} melanoma cell growth. MTX-216 treatment in NF1^{LoF} melanoma cells suppresses a group of genes that regulate mitochondrial electron transport chain and whose expression is associated with poor survival in NF1^{LoF} melanoma patients. In agreement with these findings, treatment with IACS-010759, a clinical-grade small-molecule inhibitor of the mitochondrial electron transport chain [17], also induces cell death in these cells. Therefore, the poly-selectivity of MTX-216, which includes SYK inhibition and the consequential suppression of mitochondrial electron transport chain, causes the unusually high activity of this compound in NF1^{LoF} melanoma cells, and provides a path to exploit SYK dependency to selectively block NF1^{LoF} melanoma cells.

Results

MTX-216 blocks NF1^{LoF} melanoma cell growth *in vitro* and *in vivo*

To identify actionable kinases whose inhibition might elicit efficacious anti-tumor responses in NF1^{LoF} melanoma cells, we assembled a panel of small molecule inhibitors targeting a diverse set of kinases that

act downstream or upstream of RAS signaling. The list of compounds included trametinib (a MEK1/2 inhibitor), ulixertinib (an ERK1/2 inhibitor), pictilisib (a pan-PI3K inhibitor), AZD8055 (an mTORC1/2 inhibitor), gefitinib (an EGFR inhibitor), palbociclib (a CDK4/6 inhibitor), the dual PI3K/EGFR inhibitor MTX-216 and its structural analog MTX-211 (Fig. 1a, Supplementary Fig. 1a). We used quantitative fluorescence microscopy to test the effects of these compounds, individually or in combination with one another, on cell growth and survival in a panel of nine $NF1^{LoF}$ melanoma cell lines. Among the tested cell lines, six expressed a wild-type (WT) BRAF ($BRAF^{WT}/NF1^{LoF}$), two possessed $BRAF^{V600E}/NF1^{LoF}$ double mutations, and one carried $NRAS^{Q61R}/NF1^{LoF}$ double mutations (Supplementary Fig. 1b). Each inhibitor was tested in up to four concentrations, including a maximum dose (C_{max}) of approximately 10 times the reported biochemical IC_{50} for its nominal target and additional concentrations separated by $10^{1/2}$-fold from one another. To compare inhibitor sensitivities, while correcting for differences in baseline proliferation rates among cell lines, we first calculated the average net growth rates from time-dependent changes in live cell counts following the exposure of each cell line to each inhibitor (at each dose) or vehicle (DMSO) for a period of 7 days. Normalized growth rates (i.e., DIP rates [18]) were then computed by normalizing the average net growth rate in the presence of each inhibitor to that in vehicle-treated cells (Fig. 1b, Supplementary Fig. 1c). Normalized growth rates < 0 indicated a net cell loss (i.e., cytotoxicity), a value of 0 represented no change in viable cell number (i.e., cytostasis), a value > 0 indicated a net cell gain (i.e., population growth), and a value of 1 represented cell growth at the same rate as in vehicle-treated cells (i.e., no effect). All the examined inhibitor conditions led to variable responses across $NF1^{LoF}$ cell lines. MTX-216 was, however, consistently cytotoxic, leading to steep dose-response curves and maximal effect (E_{max}) values that were significantly higher than those of trametinib and ulixertinib, the next most effective inhibitors (Fig. 1b, c).

To determine whether the superior efficacy of MTX-216 was specific to $NF1^{LoF}$ cells, we evaluated its effect on non-transformed primary melanocytes as well as on two $NF1^{WT}$/$BRAF^{V600E}$ melanoma cell lines (A375 and COLO858), that are sensitive to trametinib and ulixertinib. When tested at its highest concentration (1 μM), MTX-216 caused no cytotoxicity in primary melanocytes (Fig. 1b, d). It also exhibited a substantially less efficacious response in A375 and COLO858 cells in comparison with any of the nine $NF1^{LoF}$ cell lines tested (Fig. 1b, d).

We then asked whether the sensitivity to MTX-216 observed in $NF1^{LoF}$ cell lines was recapitulated *in vivo*. To address this question, athymic nude mice were implanted with either a slowly growing $NF1^{LoF}$ cell line (COLO792) or a rapidly growing cell line (WM3918) subcutaneously. Animals were then treated with MTX-216 (at a dose of 50 mg/kg) or vehicle by intraperitoneal injection (IP). Inhibitor administration in mice was performed every 1 to 3 days for a period of up to 20 days, during which body weight was also monitored. MTX-216 suppressed tumor growth in both cell line-derived xenograft models (Fig. 1e), while animals experienced acceptable or no loss in body weight (Supplementary Fig. 1d).

Together, these data identify MTX-216 as an efficacious agent that selectively blocks $NF1^{LoF}$ melanoma cells *in vitro* and shows encouraging signs of *in vivo* efficacy without inducing significant toxicity in non-transformed primary melanocytes. We thus set out to identify the mechanisms that might determine the anti-tumor efficacy of MTX-216 in $NF1^{LoF}$ melanomas.

MTX-216 co-suppresses Ki-67 and p-S6 and induces apoptosis in $NF1^{LoF}$ cells

To identify factors influencing the efficacy of MTX-216, we assayed apoptosis in live $NF1^{LoF}$ cells. We exposed MeWo, WM3918 and COLO792 cells to increasing concentrations of MTX-216 for 48 or 72 h. We then used the NucView® dye, a fluorogenic substrate of effector caspases 3 and 7, and measured

substrate cleavage by fluorescence microscopy [19]. Single-cell analysis revealed a dose-dependent increase in the frequency of apoptotic cells induced by MTX-216 in all three $NF1^{LoF}$ cell lines (Fig. 2a, b).

To evaluate the effect of MTX-216 on cell signaling and proliferation, we quantified dose-dependent changes in the phosphorylation state of S6 ribosomal protein ($p\text{-}S6^{S235/S236}$) and expression of Ki-67 protein by immunofluorescence microscopy. p-S6 serves as a surrogate for S6 kinase activity, integrating multiple pro-survival signals downstream of RAS signaling, including MEK/ERK and PI3K/mTOR pathways [20–22]. Ki-67 is a marker of proliferation, which is expressed at lower levels in quiescent cells than in actively proliferating cells [23]. We analyzed the single-cell expression of p-S6 and Ki-67 and their covariance in three $NF1^{LoF}$ cell lines (MeWo, WM3918 and COLO792) following 72 h treatment with either MTX-216, pictilisib, trametinib or ulixertinib. All inhibitors reduced the expression of both markers to levels that correlated with inhibitor-induced reduction of growth rate in each cell line (Fig. 2c). MTX-216, however, was the only compound that consistently drove the largest proportion of $NF1^{LoF}$ cells toward a doubly inhibited $p\text{-}S6^{Low}/Ki\text{-}67^{Low}$ state in all three cell lines (Fig. 2d and Supplementary Fig. 2). In contrast, $NF1^{WT}/BRAF^{V600E}$ COLO858 cells (which show higher dependency on MEK/ERK signaling than on PI3K/mTOR pathway and thus, greater sensitivity to MEK/ERK inhibitors than to PI3K/mTOR inhibitors) exhibited more effective co-suppression of p-S6 and Ki-67 in response to trametinib and ulixertinib in comparison with MTX-216 (Fig. 2d). Overall, these data relate the efficacious and selective inhibition of $NF1^{LoF}$ melanoma cells by MTX-216 to the ability of the compound to co-suppress Ki-67 and p-S6 at the single-cell level and the induction of apoptosis in these cells.

Inhibition of SYK by MTX-216 increases the sensitivity of $NF1^{LoF}$ cells to PI3K or MEK inhibition

To identify what is driving the high levels of efficacy following MTX-216 treatment, kinome selectivity testing was carried out against 403 human kinases using two commercial FRET-based kinase assays, including Z'-LYTE which monitors phosphorylation of peptide substrates, and Adapta that quantifies ADP formation and can be used with lipid substrates. We also tested MTX-211, a structural analogue of MTX-216, to quantify the differences in target space between the two compounds that might be responsible for their dramatically distinct effects on $NF1^{LoF}$ cells. When assayed at a concentration of 10 μM, both compounds inhibited their nominal targets, including different isoforms of the catalytic subunits of PI3K (p110α, p110β, p110δ and p110γ) and EGFR, by approximately 90-100% (Fig. 3a). The assay also identified additional kinase targets for both compounds, including mTOR, PI4KB and DNA-PK. Repeating the assay for these targets across a ~10^4-fold range of concentration showed that they were all inhibited by both compounds to similar degrees with IC_{50}'s ranging from ~0.3 nM to ~1 μM (Fig. 3b and Supplementary Fig. 3a). We hypothesized that the superior efficacy of MTX-216 might be due to inhibition of a kinase that is targeted effectively by MTX-216 but not by MTX-211. The most significant candidate was SYK, a non-receptor tyrosine kinase and an activator of RAS signaling [24,25], which was inhibited by 94% and 52% by MTX-216 and MTX-211 (both at 10 μM), respectively (Fig. 3a). Dose-response analysis revealed an IC_{50} of 281 nM for SYK kinase inhibition by MTX-216, which was >21-fold smaller than that of MTX-211 (Fig. 3c).

We then asked whether the difference in the ability of MTX-216 and MTX-211 to inhibit SYK was seen in $NF1^{LoF}$ cells when treated with these compounds. We exposed MeWo cells to MTX-216 and MTX-211 for 24 h and used Western blotting to measure dose-dependent changes in $p\text{-}SYK^{Y525/526}$, autophosphorylation sites on SYK activation loop that are required for its kinase activity [24,26]. As a control for SYK inhibition, we also tested changes in $p\text{-}SYK^{Y525/526}$ levels induced by two ATP-competitive SYK inhibitors, R406 and entospletinib [27–29]. Consistent with its higher potency in

inhibition of SYK in biochemical assays, MTX-216 reduced the levels of p-SYK$^{Y525/526}$ more effectively in comparison with MTX-211 across both tested concentrations (1 and 3.2 μM) (Fig. 3d, e). Interestingly, neither R406 nor entospletinib were able to fully inhibit p-SYK$^{Y525/526}$. The effect of MTX-216 at 1 μM, however, was comparable to that of R406, confirming the ability of MTX-216 at this concentration to inhibit SYK activity in NF1^{LoF} cells.

To test whether the difference in inhibitory effects of MTX-216 and MTX-211 on SYK kinase was recapitulated at the level of transcription, we performed RNA sequencing on two NF1^{LoF} melanoma cell lines (MeWo and WM3918) exposed to either MTX-216 (at 1 μM), MTX-211 (at 1 μM), or vehicle (DMSO) for 24 h. Genes differentially expressed by at least twofold by either MTX-216 or MTX-211 in each cell line were selected based on a statistical cutoff of FDR ≤ 0.05 (Fig. 3f). Among these genes, we focused on the subset differing in enrichment between the two compounds in both cell lines (Fig. 3g). Genes enriched specifically in MTX-216 treatment (but not in MTX-211 treatment) in both cell lines comprised 231 down-regulated genes and 467 up-regulated genes (Fig. 3h, Supplementary Fig. 3b). We used these genes in Enrichr [30] and compared them statistically with gene expression signatures extracted from the Gene Expression Omnibus (GEO) database for kinase perturbation. The top kinase perturbation term was SYK drug inhibition (Fig. 3i and Supplementary Fig. 3c), suggesting that MTX-216 (but not MTX-211) at a concentration of 1 μM affects the expression of genes, whose transcription is also influenced by SYK inhibition in a similar way.

To directly evaluate the importance of SYK for growth of NF1^{LoF} cells, we depleted the protein by siRNA in two NF1^{LoF} melanoma cell lines, MeWo and YUHEF (Fig. 4a). Following 3 and 6 days of inhibition by SYK siRNA, we measured live cell counts and computed the normalized growth rate in SYK-depleted cells relative to cells treated with non-targeting (control) siRNA. We also compared the normalized growth rates in the presence of different doses of MTX-211, trametinib and pictilisib or

vehicle (DMSO). SYK depletion in both cell lines led to a statistically significant decrease in their growth rates and enhanced their sensitivity to MTX-211, trametinib and pictilisib (Fig. 4b). We then tested the effect of SYK inhibitor R406, individually or in combination with either MTX-211, trametinib or pictilisib, on three cell lines MeWo, YUHEF, and WM3918. Inhibition of SYK by R406 reduced the growth rate in these cell lines by approximately 2-fold and enhanced their sensitivity to MTX-211, trametinib and pictilisib (Fig. 4c and Supplementary Fig. 4). Together, these data identify SYK as a target of multi-kinase inhibitor MTX-216, whose inhibition significantly decreases the growth of $NF1^{LoF}$ melanoma cells and increases their sensitivity to PI3K and MEK inhibitors.

MTX-216 suppresses genes that regulate mitochondrial electron transport chain in $NF1^{LoF}$ cells

To better understand the mechanisms underlying the superior efficacy of MTX-216 relative to other inhibitors, we extended our RNA sequencing analysis (described above) to treatments with additional inhibitors, including pictilisib (at 1 μM) and trametinib (at 0.1 μM). We also included a third $NF1^{LoF}$ cell line (SKMEL113), which was treated for 24 h with either MTX-216 (at 1 μM), trametinib (at 0.1 μM), the combination of MTX-216 and trametinib (at 1 μM and 0.1 μM, respectively), or vehicle (DMSO). We used principal component analysis (PCA) to visualize the gene expression data across 42 samples, representing 3 cell lines (MeWo, WM3918 and SKMEL113) and 6 distinct treatment conditions tested in 3 independent replicates. PCA captured >80% of variance in the entire dataset by the first five principal components (Fig. 5a). While the first two principal components (PC1 and PC2) associated mostly with cell line-specific differences, PC3 and PC4 were able to capture treatment-specific variations across the samples (Supplementary Fig. 5a). Changes induced by trametinib were revealed by a large shift in scores along PC4 for all three cell lines (Fig. 5b; purple arrows). MTX-216 treatment, on the other hand, led to a moderate shift along PC4, while inducing a strong shift along PC3 (Fig. 5b; blue

arrows). The combination of trametinib and MTX-216 was additive, leading to substantial shifts in both PC4 and PC3 (Fig. 5b; red arrow), whereas pictilisib and MTX-211 induced only small changes along both principal components.

Because PC3 and PC4 separated the efficacious inhibitors independent of cell lines, we set out to use PC3 and PC4 loadings to identify genes associated with distinct inhibitory effects on $NF1^{LoF}$ cells. Gene loadings that were differentially enriched along either PC3 or PC4 were selected based on a ratio cutoff of *cotangent* ($\pi/8$) ≈ 2.4 (Fig. 5c). Among these genes, we focused on the subsets along each PC that had loading values of greater than 1.5×median for positive loadings, or smaller than 1.5×median for negative loadings (Fig. 5c). The selected genes comprised 315 genes with strong positive PC3 loadings, 414 genes with strong negative PC3 loadings, 491 genes with strong positive PC4 loadings, and 678 genes with strong negative PC4 loadings. The top Gene Ontology (GO) terms associated with significantly negative PC4 loadings included processes involved in cell cycle progression, DNA replication and mitosis (Fig. 5d; blue bars). As expected from the PCA scores, these genes were suppressed profoundly in cells exposed to trametinib but were also down-regulated in cells treated with MTX-216 (Supplementary Fig. 5b). In contrast, genes associated with negative PC3 loadings were substantially down-regulated only in MTX-216 treated cells, but not in cells treated with other inhibitors (Supplementary Fig. 5b). The top GO terms associated with these genes included processes involved in cellular respiration and oxidative phosphorylation such as mitochondrial ATP synthesis and respiratory electron transport chain complex biogenesis and assembly (Fig. 5d; red bars). Consistent with these results, an independent gene set enrichment analysis (GSEA) using consolidated Hallmark gene sets [31] identified oxidative phosphorylation to be significantly associated with genes down-regulated by MTX-216 (Fig. 5e). Among the key genes affected were those that encode mitochondrial enzyme subunits involved in the respiratory electron transport chain, such as NADH:Ubiquinone Oxidoreductase

Subunits A1 and B1(NDUFA1, NDUFB1), Ubiquinol-Cytochrome C Reductase Complex III Subunit VII (UQCRQ) and Cytochrome C Oxidase Subunit 5A (COX5A), which were all consistently down-regulated by MTX-216, but not by trametinib, in all three cell lines (Fig. 5f). Proliferation hallmarks (such as E2F targets, MYC targets and G2/M checkpoint), however, were down-regulated by both trametinib and MTX-216 (Fig. 5e, Supplementary Fig. 5c). Together, these data show that while both MTX-216 and trametinib are effective in inhibition of cell proliferation in $NF1^{LoF}$ melanoma cells (as demonstrated above by Ki-67 analysis and growth rate inhibition assays), the two compounds are distinguishable with respect to their effect on the suppression of genes that regulate mitochondrial electron transport chain.

Mitochondrial respiratory chain is associated with poor survival in $NF1^{LoF}$ melanomas patients and inhibitable by MTX-216 or SYK inhibition

To test the clinical relevance of genes encoding mitochondrial electron transport chain (ETC) in $NF1^{LoF}$ melanoma tumors, we assessed their association with patient survival using The Cancer Genome Atlas (TCGA) database. We used summed z-score values for the respiratory ETC GO term (including 116 genes) to stratify tumors derived from 339 melanoma patients into subgroups of ETC^{High} versus ETC^{Low} in an unbiased manner (Supplementary Fig. 6a). Among the 48 NF1-mutant melanoma patients in this population, 19 were classified as ETC^{High} and had a significantly shorter overall survival compared to the remaining 29 patients who were classified as ETC^{Low} (log-rank FDR = 0.02) (Fig. 6a). We then asked whether the ETC signature correlated with patient survival in $NF1^{WT}$ tumors driven by other MAPK mutations, including BRAF and NRAS mutations. Interestingly, we did not observe a significant association between the overall survival and whether tumors belonged to ETC^{High} or ETC^{Low} subgroups in $NF1^{WT}$ patients carrying BRAF or NRAS mutations (Fig. 6b, c).

To directly evaluate the importance of the mitochondrial respiratory chain for growth of $NF1^{LoF}$ cells, we used IACS-010759, a clinical-grade small molecule inhibitor of complex I of the mitochondrial electron transport chain. We exposed $NF1^{LoF}$ cell lines, MeWo and WM3918, to a range of IACS-010759 concentrations. IACS-010759 inhibited proliferation and induced cell death in both cell lines (Fig. 6d), supporting the hypothesis that $NF1^{LoF}$ cells depend on mitochondrial respiratory chain for growth and survival.

Because genes down-regulated by MTX-216 were involved in the mitochondrial respiratory chain, we asked whether this effect was due to a global reduction in mitochondrial mass or function because of SYK inhibition by this compound. We thus used the fluorescent probes, MitoTracker Deep Red and MitoTracker Red CMXRos, to quantitate the mitochondrial mass and mitochondrial membrane potential in $NF1^{LoF}$ cells, respectively [32]. Measurements were performed by fluorescence microscopy in two cell lines (MeWo and WM3918) following treatment with either MTX-216 (at 1 μM) or vehicle (DMSO) for 48 h, or with SYK siRNA or a non-targeting control siRNA for 72 h. Both SYK knockdown (Fig. 6e, f) and MTX-216 treatment (Fig. 6g, h, Supplementary Fig. 6b) shifted cell populations towards lower levels of both mitochondrial markers. Together, these results are consistent with RNA sequencing data, suggesting that the efficacy of MTX-216 through SYK inhibition is mediated by the suppression of mitochondrial mass and mitochondrial electron transport chain function, whose elevation appears to be associated with shorter overall survival in $NF1^{LoF}$ melanoma patients.

Discussion

The loss of function of NF1 is among oncogenic events that amplify the physiological control mechanisms of RAS signaling and cause the activation of multiple downstream signaling pathways such as MEK/ERK, PI3K/mTOR and other pro-survival pathways [13]. This has made it difficult to find an

effective targeted therapy for melanomas driven by $NF1^{LoF}$ mutations. To begin to address this challenge, we performed a kinase inhibitor screen to identify vulnerabilities, whose inhibition individually or in combination with MEK/ERK or PI3K/mTOR inhibitors would be effective in blocking $NF1^{LoF}$ melanoma cells. We found that the efficacy of kinase inhibitors in suppressing proliferation and inducing cell death was highly correlated with their ability to co-inhibit the proliferation marker Ki-67 and the ribosomal S6 phosphorylation (p-S6), an integrator of multiple RAS-mediated signaling pathways. While MEK/ERK inhibitors and PI3K inhibitors led to heterogeneous responses, we identified a new compound, MTX-216, that effectively suppressed both Ki-67 and p-S6 in $NF1^{LoF}$ melanoma cells and induced efficacious cytotoxic responses in these cells. MTX-216 was developed as a dual ATP-competitive inhibitor of PI3K isoforms and EGFR. However, systematic analysis of the effect of this compound on kinome and transcriptome showed that its higher efficacy in $NF1^{LoF}$ cells compared to MTX-211 (a structural analogue of MTX-216 which also inhibits PI3K and EGFR) depended on its unique ability to inhibit SYK kinase. In multiple $NF1^{LoF}$ melanoma cell lines, combinations of inhibitors targeting either MEK or PI3K/mTOR with an independent SYK kinase inhibitor (R406) or SYK knockdown also showed favorable effects. Therefore, the study of MTX-216 served as a tool to identify SYK as a new vulnerability which when exploited in combination with MEK or PI3K/mTOR inhibition can lead to efficacious responses in $NF1^{LoF}$ melanoma cells.

It is expected that the lack of negative regulation on RAS makes $NF1^{LoF}$ cells sensitive to inhibitors of RAS activators [13]. In contrast, $BRAF^{V600E}$ cells have substantially low RAS activity, due to profound feedback inhibition, and thus do not show sensitivity to inhibitors of RAS activators [33]. The greater efficacy of MTX-216 in $NF1^{LoF}$ cells, in comparison with $BRAF^{V600E}$ cells, is thus consistent with this compound being able to inhibit SYK, a non-receptor tyrosine kinase that can be activated by multiple upstream receptors and initiates downstream signaling through RAS [24,25,34–36]. Nevertheless, our

data prompt additional future investigations to more fully define the role of SYK and its associated adaptors in downstream RAS signaling and how they are mechanistically linked to oncogenesis in $NF1^{LoF}$ melanomas.

Our transcriptomic analysis provides insight into how MTX-216 promotes anti-tumor effects in $NF1^{LoF}$ melanoma cells by suppressing a group of genes that regulate mitochondrial electron transport chain and function. The expression of these genes is associated with poor survival in patients with $NF1^{LoF}$ melanomas, but not in patients with BRAF-mutated or NRAS-mutated tumors. Therefore, MTX-216 may block $NF1^{LoF}$ melanoma cells by targeting a mitochondrial vulnerability associated with a specific SYK-dependent signaling context in these cells. This is consistent with the sensitivity of $NF1^{LoF}$ melanoma cells to pharmacological inhibition of mitochondrial electron transport chain either by IACS-010759 as demonstrated in this study, or by phenformin as reported previously [11]. It also agrees with previous reports linking the SYK pathway activity to the mitochondrial respiratory chain function in diverse cell types [16]. Furthermore, the anti-tumor effect of SYK inhibition in other SYK-dependent malignancies, such as acute myeloid leukemia and diffuse large B cell lymphoma, is also mediated through the suppression of mitochondrial biogenesis and oxidative metabolism [37–39]. Future studies may leverage these findings to elucidate the mechanistic connection between SYK pathway activity and mitochondrial function in $NF1^{LoF}$ melanomas.

MTX-216, the tool compound used in this study, was originally developed as a dual inhibitor of PI3K and EGFR, and thus its ability to inhibit SYK was not intentional. Furthermore, the phenotypic consequences of SYK inhibition could not have been predicted but appeared to be highly effective in $NF1^{LoF}$ cells. Hence, the discovery of SYK as a vulnerability in $NF1^{LoF}$ melanomas represents an unconventional approach leveraging mechanistic, poly-pharmacology drug studies to identify novel cancer targets [15]. There are many instances of kinase inhibitors (including clinically approved therapies

such as sorafenib), whose anti-tumor efficacy was found to be due to their ability to inhibit kinases other than their originally intended targets [40–43]. This is not surprising because all kinases bind to a common substrate (i.e., ATP), which underlies their great potential for promiscuity. Therefore, individual kinase inhibitors may have many unpredicted target combinations, leading to unique biological activities that could be exploited to discover new mechanisms as well as novel actionable dependencies in cancer cells. The discovery of SYK dependency in $NF1^{LoF}$ melanoma cells in this study is an example of such discoveries that warrants further mechanistic investigation to better understand the role of SYK in $NF1^{LoF}$ melanomas in future studies. Such studies may provide a path to exploit SYK dependency to selectively block $NF1^{LoF}$ melanoma tumors.

Methods

Cell lines and reagents

Melanoma cell lines used in this study were obtained from the following sources: LOXIMVI (from DCTD Tumor Repository, National Cancer Institute), COLO858 and COLO792 (from ECACC), MeWo and A375 (from ATCC), SKMEL113 (from Memorial Sloan-Kettering Cancer Center), WM3918 (from Rockland Immunochemicals), human epidermal primary melanocytes (NHEM-Ad; from Lonza), YUHEF, YURED, YUHOIN, and YUTICA (all from Yale University Dermatology Cell Culture Facility). All of the cell lines have been periodically subjected to re-confirmation by Short Tandem Repeat (STR) profiling by ATCC and mycoplasma testing by MycoAlert™ PLUS mycoplasma detection Kit (Lonza). YUHEF, YURED, YUHOIN, and YUTICA cells were grown in Opti-MEM (Gibco, Cat# 31985088) supplemented with 5% fetal bovine serum (FBS). COLO858, LOXIMVI, COLO792, and SKMEL113 cells were grown in RPMI 1640 (Corning, Cat# 10-040-CV) supplemented

with 1% Sodium Pyruvate (Invitrogen) and 5% FBS. A375 cells were grown in DMEM with 4.5 g/L glucose (Corning, Cat# 10-013-CV) supplemented with 5% FBS. MeWo cells were grown in EMEM (Corning, Cat# 10-009-CV) supplemented with 5% FBS. WM3918 cells were grown in 80% MCDB 153 (Sigma-Aldrich, Cat# M7403), 20% Leibovitz's L-15 (Sigma-Aldrich, Cat# L1518), 5% FBS, and 1.68 mM $CaCl_2$. NHEM-Ad cells were grown in MGM-4 Melanocyte Growth Medium-4 BulletKit (Lonza, Cat# CC-3249). We added penicillin (50 U/mL) and streptomycin (50 lg/mL) to all growth media.

Small molecule inhibitors trametinib, ulixertinib, AZD8055, palbociclib, gefitinib, pictilisib, entospletinib, R406 and IACS-010759 were all purchased from Selleck Chemicals. MTX-216 and MTX-211 were synthesized by Albany Molecular. MTX-211 (HY-107364) is also available from MedChemExpress. Compounds used for cell-based studies were dissolved in the appropriate vehicle (DMSO) at a stock concentration of 5 or 10 mM.

The following primary monoclonal antibodies (mAb) and polyclonal antibodies (pAb) with specified animal sources, catalogue numbers and dilution ratios, were used in immunofluorescence staining and Western blot assays : Ki-67 (mouse mAb, Cell Signaling Technology, Cat# 9449, 1:800), p-$S6^{S235/S236}$ (rabbit mAb, Cell Signaling Technology, Cat# 4851, 1:400), SYK (mouse mAb, Santa Cruz Biotechnology, Cat# 1240, 1:1000), p-$SYK^{Y525/526}$ (rabbit mAb, Cell Signaling Technology, Cat# 2710, 1:1000), and β-tubulin (rabbit pAb, Cell Signaling Technology, Cat# 2146, 1:1000). The following secondary antibodies with specified sources and catalogue numbers were used at 1:2000 dilution for immunofluorescence assays: anti-mouse Alexa Fluor 488 (Thermo Fisher, Cat# A21202) and anti-rabbit Alexa Fluor 647 (Thermo Fisher, Cat# A31573). The following secondary antibodies with specified sources and catalogue numbers were used at 1:15000 dilution for Western blot assays: anti-rabbit IRDye

800CW (LI-COR Biosciences, Cat# 926-32213) and anti-mouse IRDye 680RD (LI-COR Biosciences, Cat# 926-68072).

Measurements of normalized growth rate and drug sensitivity

Growth rate inhibition assays with kinase inhibitors were performed in 96-well clear bottom black plates (Corning, Cat# 3904). Viable cells were counted using a TC20 automated cell counter (Bio-Rad Laboratories) and seeded in 200 µL of full growth media at a density of 1,700-2,500 cells per well, depending on the baseline proliferation rate of each cell line. Cells were treated the next day with small molecule compounds at reported concentrations or with vehicle control (DMSO) using a D300e Digital Dispenser. Live cells were counted across timepoints: t = 24, 72, 120 and 168 h, and used to calculate net growth rates across treatments. All treatments across different inhibitor concentrations and timepoints were performed in duplicate. At designated timepoints, cells were fixed with 4% paraformaldehyde (PFA) for 20 min at room temperature. Cells were then washed twice with PBS and stained with Hoechst 33342 (Thermo Fisher, Cat# H3570, 1:20000) for 20 min at room temperature. Cells were washed twice with PBS and imaged with a 10x objective using the ImageXpress Micro Confocal High-Content Imaging System (Molecular Devices) or the Operetta CLS High-Content Imaging System (Perkin Elmer). A total of 9 sites were imaged per well. Background subtraction was performed with ImageJ v.2.1.0 software. Nuclear segmentation to generate cell count data was performed using CellProfiler v.3.1.9 software [44]. All follow-up computational and statistical analysis was performed using MATLAB 2019b software.

The net growth rate for cells treated with individual compounds (at different doses), or their combination, or vehicle, was calculated from time-dependent changes in live cell count according to the following equation:

$$k = \frac{ln\left(\frac{N_{t2}}{N_{t1}}\right)}{t_2 - t_1} \qquad (1)$$

where N_{t1} and N_{t2} represent the number of cells measured at timepoints $t = t_1$ and $t = t_2$, respectively, and k describes the net growth rate of cells during the time period between t_1 and t_2. The net growth rates were then averaged across multiple, consecutive time intervals to determine the mean net growth rate for each condition. To compare drug sensitivity among different cell lines, we corrected for their differences in their baseline proliferation rates by normalizing the mean net growth rate measured for drug-treated cells (k_{drug}) to that measured for vehicle (DMSO)-treated cells (k_{DMSO}) to calculate the drug-induced normalized growth rate (a.k.a. DIP rate [18]):

$$Normalized\ growth\ rate = \frac{k_{drug}}{k_{DMSO}} \qquad (2)$$

Normalized growth rates < 0 indicate a net cell loss (i.e. cytotoxicity), a value of 0 represents no change in viable cell number (i.e. cytostasis), a value > 0 indicates a net cell gain (i.e. population growth), and a value of 1 represents cell growth at the same rate as in DMSO-treated (control) cells.

Immunofluorescence staining, quantitation, and analysis

Cells in Corning 96-well plates were fixed with 4% PFA for 20 min at room temperature at designated timepoints (24 to 168 h). Cells were then washed twice with PBS, and then permeabilized in 100% ice-cold methanol for 10 min at -20° C. Cells were rewashed with PBS and blocked using Odyssey Blocking Buffer (LI-COR) for 1 h at room temperature. Cells were then stained with primary antibodies at their appropriate dilutions in Odyssey Blocking Buffer overnight (~16 h) at 4° C. The next day, cells were washed three times with PBS supplemented with 0.1% Tween-20 (Sigma-Aldrich) (PBS-T). Cells were then stained with secondary antibodies for 1 h at room temperature followed by washing once with PBS-T, once in PBS, and incubated with Hoechst 33342 for 20 min at room temperature. Cells were

washed twice with PBS and imaged with a 10x objective using the ImageXpress Micro Confocal High-Content Imaging System (Molecular Devices) or the Operetta CLS High-Content Imaging System (Perkin Elmer). A total of 9 sites were imaged per well. Background subtraction was performed with ImageJ v.2.1.0. Image segmentation and signal intensity quantification was performed with CellProfiler v.3.1.9. Single-cell data were analyzed using MATLAB 2019b. By generating histograms of single-cell data across a variety of conditions for each protein (X), including positive and negative controls, we identified an appropriate binary gate, based on which the percentage of X^{High} versus X^{Low} cells in each condition was quantified.

Apoptosis assay

COLO792 and MeWo cells were seeded in 96-well clear bottom black plates in full phenol red free growth media (100 µL/well). WM3918 were seeded in their usual full growth media. Cells were treated the next day with indicated concentrations of MTX-216 (in duplicate) using D300e Digital Despenser. After 48 or 72 h of treatment, a reagent cocktail comprised of Hoechst 33342 and NucView 488 Caspase-3 reporter (Biotium, Cat# 30029) was added to each well for final concentrations of 1 µg/mL and 1 µM, respectively. The plates were then incubated in a tissue culture incubator (37°C, 5% CO2) for 1.5 h. Pre-warmed PFA was then added to each well for a final concentration of 1%. Plates were then sealed using Microseal aluminum foil (Bio-Rad), incubated for 30 min at room temperature and imaged with a 10x objective using the ImageXpress Micro Confocal High-Content Imaging System. Background subtraction was performed with ImageJ v.2.1.0 and single-cell segmentation and signal intensity quantification was performed on CellProfiler v.3.1.9. Single-cell data were analyzed using MATLAB 2019b software. By generating histograms of single-cell data across a variety of conditions

for NucView staining, including positive and negative controls, we identified an appropriate binary gate, based on which the percentage of apoptotic (NucView ^{High}) cells in each condition was quantified.

Biochemical kinase inhibition assays

To assess their ability to inhibit each of 403 human kinases, MTX-216 and MTX-211 were outsourced to SelectScreen Biochemical Kinase Profiling service at ThermoFisher. Each compound was screened at 10 µM using either Z'-LYTE or Adapta kinase activity assay at an ATP concentration of $K_{m,app}$ for each target. The Z'-LYTE assay monitors phosphorylation of peptide substrates, and Adapta quantifies ADP formation and thus can be used with lipid substrates. For selected targets that were inhibited significantly (>90%) by MTX-216 or MTX-211 at 10 µM (e.g., SYK), we repeated the kinase activity assay across 10 concentrations (using 3-fold serial dilutions). Dose-response plots and the corresponding IC_{50}'s were generated using the function doseResponse (developed by Ritchie Smith) available on the MATLAB Central File Exchange (https://www.mathworks.com/matlabcentral/fileexchange/33604-doseresponse).

Gene knockdown by siRNA

siRNA knockdown experiments with MeWo and YUHEF cells were performed in antibiotic-free growth media either in cells seeded in 10-cm plates (for the purpose of Western blotting) or in Corning 96-well clear bottom black plates (at a density of 2,500 and 1,000 cells/well, respectively) for the purpose of cell counting and inhibitor sensitivity analysis. In both cases, 24 h after cell seeding, cells were transfected with Dharmacon's ON-TARGETplus Human SMARTpool siRNA for SYK (L-003176-00-0005), or non-targeting control (D-001810-10-05) at 25 nM each. The SMARTpool siRNA included four SYK-specific siRNAs combined into a single pool to increase the likelihood of effective gene silencing.

DharmaFECT 2 (GE Dharmacon, Cat# T-2002-01) and DharmaFECT 3 (GE Dharmacon, Cat# T-2003-01) were used as transfection reagents for MeWo and YUHEF cells, respectively. After 72 h of culture in the presence of siRNAs, cells in 10-cm plates were transferred to ice, washed with ice-cold PBS, and lysed for the purpose of Western blotting. After 72 h of knockdown, cells in 96-well plates were either fixed with 4% PFA or treated with kinase inhibitors (trametinib, MTX-211, pictilisib) or DMSO for an additional 72 h before fixation. All fixed cells were then stained with Hoechst 33342 and counted using quantitative immunofluorescence microscopy. Time-dependent changes in cell count were used to compute normalized growth rates as described above. All knockdown experiments were performed in triplicate.

Western blots

Following 72 h of culture in the presence of siRNAs or 24 h after treatment with indicated inhibitors, cells were transferred to ice, washed with ice-cold PBS, and lysed with ice-cold RIPA buffer (Thermo Fisher, Cat# 89901) consisting of 25 mM Tris-HCl (pH 7.6), 150 mM NaCl, 1% NP-40, 1% sodium deoxycholate, and 0.1% SDS supplemented with 1 mM Na_3VO_4, 15 mM NaF, cOmplete ULTRA EDTA-free protease inhibitors (Roche, Cat# 5892953001) and PhosSTOP (Roche, Cat# 4906837001). Protein samples of cleared lysates were measured using BCA assay (Thermo Scientific, Cat# PI23235). Lysates were adjusted to equal protein concentrations for each treatment condition, 4× NuPage LDS sample buffer (Invitrogen, Cat# NP0007) supplemented with 1 µL of 1 M DTT was added, and samples were heated for 10 min at 70°C. Samples were then loaded on NuPAGE 3-8% Tris-Acetate gels (Invitrogen). Western blots were performed using iBlot 2 Gel Transfer Stacks PVDF system (Invitrogen). Membranes were blocked with Intercept (TBS) Blocking Buffer (LI-COR, Cat# 927-60001) for 1 h and then incubated with primary antibodies (1:1000 dilution) in 0.5x Intercept blocking

buffer solution (diluted with TBS, supplemented with 0.1% Tween-20) overnight at 4° C. Secondary antibodies were used at 1:15000 dilution in 0.5x Intercept blocking buffer solution supplemented with 0.01% SDS. Membranes were scanned on an Odyssey CLx scanner (LI-COR) with 700 and 800 nm channels set to automatic intensity at 169 µm resolution. Blot images were processed, on Image Studio Lite v.5.2.5 software (LI-COR).

MitoTracker staining, imaging and quantitation

Cells were seeded at 100 µL/well in 96-well PerkinElmer ViewPlates (PerkinElmer, Cat# 6005225). Cells were treated the next day with either SYK siRNAs (or non-targeting control) or 1 µM MTX-216 (or DMSO) in triplicate. At the designated timepoints (72 h in case of siRNA knockdown and 48 h in case of inhibitor treatments), MitoTracker Deep Red (Invitrogen, Cat# M22426) and MitoTracker Red CMXRos (Invitrogen, Cat# M7512) were added to the wells for a final concentration of 100 nM for each dye. The plates were then incubated in a tissue culture incubator (37°C, 5% CO2) for 45 min. The media including dye solution were aspirated, wells were washed with pre-warmed media (including inhibitor or DMSO), and placed in incubator for 1 h to wash out nonspecific binding of dye. Cells were then washed with PBS followed by 4% PFA fixation for 15 min at room temperature. Plates were washed three times (5 min each) with PBS followed by Hoechst 33342 staining for 20 min. Plates were washed twice with PBS and sealed using Microseal aluminum foil (Bio-Rad). Plates were imaged with 20x water-immersion objective using the Operetta CLS High-Content Imaging System (Perkin Elmer). A total of 37 sites were imaged per well. Background subtraction was performed with ImageJ v.2.1.0. Image segmentation and signal intensity quantification was performed with CellProfiler v.4.0.7. Single-cell data were analyzed using MATLAB 2020b software.

***In vivo* xenograft assays**

Animal handling, care and treatment was carried out in accordance with procedures approved by the Institutional Animal Care and Use Committee (IACUC) at the University of Michigan. For the COLO792 xenograft studies, female 5-6 weeks old NCR nude mice (Taconic, CrTac:NCr-*Foxn1*^{nu}) were implanted subcutaneously with 2.5×10^6 cells in 1:1 Matrigel:serum-free media. When the average tumor volume was approximately 125 mm^3 (on day 39 post-implantation), mice were randomized into treatment groups and treatments were initiated. MTX-216 was prepared fresh daily as a clear solution in 1:2 propylene glycol:1% Tween80/Na_3PO_4, and administered intraperitoneally (IP) based upon individual animal body weight (0.2 mL/20 grams) on days 1 (i.e., day 39 post-implantation), 2, 4, 7, 10, 13 and 16. Tumor volumes were measured on days 1, 3, 6, 8, 12, 15, 18, and 20 post-treatment. Tumor volumes were calculated by measuring two perpendicular diameters with calipers and using the formula: tumor volume (mm^3) = (length × $width^2$)/2. Animal body weights were measured two to three times a week. At the completion of the experiment, the mice were euthanized.

For the WM3918 xenograft studies, female 5-6 weeks old NCR nude mice (Taconic) were implanted subcutaneously with 1.5×10^6 cells in 1:1 Matrigel:serum-free media. When the average tumor volume was approximately 115 mm^3 (on day 6 post-implantation), mice were randomized into treatment groups and treatments were initiated. MTX-216 was prepared fresh daily as a fine, light brown homogenous suspension including 5% DMSO and 95% PBS with a pH of 7. MTX-216 was administered once daily intraperitoneally (IP) based upon individual animal body weight (0.2 mL/20 grams), beginning on day 1 (i.e., day 6 post-implantation). Tumor volumes were measured on days 1, 3, 5, 7, 9 and 11. Animal body weights were measured two to three times a week. Mice continued to receive daily treatments until vehicle-treated tumor volume exceeded 1,000 mm^3 (day 11). At this time, mice were euthanized.

RNA extraction, library construction, and RNA sequencing analysis

MeWo, WM3918, and SKMEL113 cells were seeded in 10-cm plates in three replicates, and treated the next day with either DMSO, MTX-216 (at 1 μM), MTX-211 (at 1 μM), pictilisib (at 1 μM), trametinib (at 0.1 μM), or the combination of MTX-216 (at 1 μM) and trametinib (at 0.1 μM), for 24 h. At the time of harvest, cells were washed once with PBS and then lysed with Rneasy Buffer RLT (Qiagen) in the dish. Lysate samples were then vortexed and frozen. To extract RNA, lysate samples were thawed at room temperature and then processed using QIAshredder (Qiagen, Cat# 79654) and Rneasy Mini Kit (Qiagen, Cat# 74104). RNA was Dnase treated (Qiagen, Cat# 79254) and then eluted. RNA quality was assessed by Bioanalyzer (Agilent). All samples had RINs of 9.0 or higher. Prior to poly-A enrichment, 500 ng of each RNA sample was supplemented with 1 μL (1:100 dilution) of ERCC spike-in control (Life Technologies, Cat# 4456740). Poly-A RNA enrichment was performed using NEBNext Poly(A) kit (New England BioLabs). Fragments were end-modified with adaptors using NEBNext Multiplex Oligos for Illumina Set 2 (New England BioLabs), following library amplification (PCR, 11 cycles). Resulting libraries were prepared using NEBNext Ultra II Directional RNA Kit (New England BioLabs). Samples were run on Illumina NovaSeq (S4) using paired-end read with 150 cycles. In total, 1.4 billion reads were generated, including ~33 million reads per sample. Reads were mapped to the human genome (hg38) using HISAT2 [45], transcripts were assembled and quantified using StringTie [46,47], and differential gene expression analysis was performed by DESeq2 using the web-based Galaxy platform (https://usegalaxy.org/) [48,49].

To identify genes regulated uniquely by MTX-216 versus MTX-211 in WM3918 and MeWo cells, we first selected those genes with base mean ≥ 1, that changed in abundance by more than twofold relative to a DMSO-treated control ($|\log_2(\text{fold change})| \geq 1$; FDR < 0.05) in each cell line. Among these

genes, we then identified the subset that was similarly up- or down-regulated by each compound in both cell lines. Genes enriched specifically by MTX-216 treatment (but not in MTX-211 treatment) in both cell lines were used in Enrichr (https://maayanlab.cloud/Enrichr/) [30] and compared statistically with gene expression signatures extracted from the Gene Expression Omnibus (GEO) database for kinase perturbation [50].

To systematically perform differential gene expression analysis across three cell lines treated with different compounds (MTX-216, MTX-211, pictilisib, trametinib, MTX-216 plus trametinib, or DMSO), we used principal component analysis (PCA). For PCA, we first organized the gene expression dataset into a matrix with 42 rows (representing 3 cell lines, 6 distinct treatment conditions, and 3 independent replicates) and 16,940 columns (representing genes). The list of these genes was generated after filtering out transcripts with unidentified gene names and functions in StringTie and removing those genes for which all 42 conditions had TPM values < 1. Then $\log_2(\text{TPM}+1)$ values were calculated for each gene and z-scored across all 42 conditions. PCA was then performed using the MATLAB built-in function pca.

Because PC3 and PC4 separated the efficacious inhibitors independent of cell lines, we used PC3 and PC4 loadings to identify genes associated with distinct inhibitory effects on cells treated with different compounds. Gene loadings that were differentially enriched along either PC3 or PC4 were selected based on a ratio cutoff of *cotangent* $(\pi/8) \approx 2.4$. Among these genes, we identified the subsets along each PC that had loading values of greater than 1.5×median for positive loadings, or smaller than 1.5×median for negative loadings. These genes were then used in Enrichr to identify significant Gene Ontology (GO) Biological Processes.

Hierarchical clustering

Following PCA, unsupervised hierarchical clustering of expression levels of genes with negative PC3 or PC4 loadings was carried out using MATLAB 2020b with the Euclidean distance metric and the Average linkage algorithm for computing the distance between clusters.

Gene set enrichment analysis

Gene set enrichment analysis (GSEA) [51,52] was performed using GSEA v.4.1.0 software and the GSEAPreranked module. Genes were pre-ranked based on their $\log_2$-fold change of expression (by MTX-216 or trametinib relative to DMSO) and *P* values generated from DESeq2 for three replicates in each of the three cell lines tested (MeWo, WM3918 and SKMEL113) using the following equation:

$$R_i = -log_{10}P_i \times sign[f_i] \quad (3)$$

where R_i represents the rank for gene *i*, P_i represents the *P* value associated with change of expression for gene *i*, and f_i represents the log2 fold change associated with gene *i*. GSEA was performed with 1,000 permutations across Hallmark gene sets [31] to determine downregulated and upregulated biological pathways.

The Cancer Genome Atlas (TCGA) bioinformatics analysis

The clinical history and the corresponding gene expression (HTSeq Counts) data from patients enrolled in the Skin Cutaneous Melanoma (SKCM) project of the TCGA [1] were accessed using the cBio Cancer Genomics Portal [53] (http://cbioportal.org/) and the Genomic Data Commons Data Portal (https://portal.gdc.cancer.gov/). A total of 339 melanoma tumors with putative driver mutations in BRAF (197 samples), NRAS (94 samples) and NF1 genes (48 samples) were identified. Tumors with double mutations in both BRAF and NF1 or in both NRAS and NF1 were included in the NF1-mutated cohort. We used summed z-score values across 116 genes of the Respiratory Electron Transport Chain

GO term (http://geneontology.org/) to stratify each of the 339 tumors into two subgroups, ETC^{High} and ETC^{Low}, based on summed z-score of > 0 and < 0, respectively. We then used the tumors with ETC^{High} and ETC^{Low} signatures in each mutation cohort (BRAF, NRAS and NF1) to compare the overall patient survival between each subgroup based on two-sided *P* values computed by log-rank (Mantel-Cox) test. *P* values were then corrected using the Benjamini-Hochberg FDR procedure.

Statistics and reproducibility

No statistical method was used to predetermine sample size. Sample sizes were chosen based on similar studies in the relevant literature. The experiments were not randomized. The investigators were not blinded to allocation during experiments and outcome assessment. All data with error bars were presented as mean values ± s.d. or mean values ± s.e.m. as indicated in figure legends using indicated numbers of independent replicates. The significance of pairwise correlations among drug response data were evaluated based on *P* values associated with the corresponding two-sided Pearson's correlation analysis (*r* = correlation coefficient). To identify the statistical significance of differences between mean of measurements within two different groups (e.g., the effect of SYK inhibitor or SYK siRNA on the growth rate of melanoma cells or MitoTracker staining), *P* values from two-sided *t* test were used. Statistical significance of the difference in % change in tumor size in mouse experiments or the effect of SYK siRNA or SYK inhibitor on responses of melanoma cells to MTX-211, pictilisib and trametinib were determined by two-way analysis of variance (ANOVA). Statistical analyses were performed using MATLAB 2020b software.

Data availability

All data generated in this study are included in this manuscript or its supplementary information files

and the raw sequencing datasets will be deposited into Gene Expression Omnibus (GEO).

Code availability

Data analysis was performed in MATLAB using built-in functions and parameters as described in Methods. Scripts are available upon request.

Materials Availability

All cell lines and reagents used in this study are available via commercial or non-commercial resources described, except for MTX-216, which is currently available upon request from Judith Sebolt-Leopold (jssl@med.umich.edu).

Acknowledgments

We thank the University of Virginia Advanced Microscopy Facility, University of Michigan Advanced Genomics Core, Kevin Janes, David Kashatus, Jennifer Kashatus, Armand Bankhead and members of the Fallahi-Sichani laboratory for help and discussion. This work was supported by the Turner-McConnell Fund for Drug Discovery of the University of Michigan Rogel Cancer Center, Department of Defense PRCRP Career Development Award W81XWH1810427 (to MFS), and NIH grants R01-CA249229 (to MFS) and R01 grants CA220199 and CA241764 (to JSL). JSL was also supported by UMCCC Core Grant P30 CA046592.

Author Contributions

C.A., C.W., E.Z., D.G.B. and C.F.-M. generated reagents, performed the experiments and analyzed the experimental data. C.A. performed bioinformatics and statistical analyses. C.A. and M.F.-S. wrote the

manuscript. All authors reviewed and assisted with manuscript preparation. M.F.-S. conceived the project. M.F.-S. and J.S.-L. supervised the work.

State of Competing Interests

C.W. is a cofounder of Mekanistic Therapeutics and has ownership interest in the same. J.S.-L. is a cofounder of Mekanistic Therapeutics and has ownership interest in the same. The other authors declare that they have no competing interests.

Figure Legends

Figure 1. MTX-216 blocks tumor growth in NF1^{LoF} melanomas *in vitro* and *in vivo*. (a) A simplified schematic illustration of the function of NF1 in the context of RAS-mediated activation of ERK and PI3K/mTOR signaling in response to upstream growth factors. The nominal targets for kinase inhibitors tested in this study are highlighted. **(b)** Dose-dependent changes in normalized growth rates (a.k.a. DIP rates) calculated by dividing the 7-day average net growth rate for inhibitor-treated cells to that measured for vehicle (DMSO)-treated cells across cell lines with different NF1/BRAF/NRAS mutation status or primary epidermal melanocytes. The average net growth rates for each condition were calculated from measurements of live cell count (across two replicates) at four timepoints (including 1, 3, 5, and 7 days). Normalized growth rates < 0 indicate a net cell loss (i.e., inhibitor-induced cytotoxicity), a value of 0 represent no change in viable cell number (i.e., cytostasis), a value > 0 indicates a net cell gain, and a value of 1 represents no effect as cells grow in the presence of inhibitor at the same rate as in the DMSO condition. **(c, d)** Inhibitor maximal effect (E_{max}), defined as the normalized growth rate evaluated at the highest tested concentration, of different inhibitors across NF1^{LoF} melanoma cell lines **(c)** and between NF1^{LoF} cell lines and NF1^{WT} cells, including two

BRAF^{V600E} melanoma cell lines and primary melanocytes **(d)**. Statistical significance was determined by two-sided, paired-sample *t* test **(c)** or two-sided, two-sample *t* test **(d)**. **(e)** Mice bearing xenografts of COLO792 cells (top) and WM3918 cells (bottom) were treated with MTX-216 or vehicle for a period of 20 and 11 days, respectively, to determine the effect on tumor growth. Tumor volume data represent mean values ± s.e.m across 4 mice per group (in case of COLO792) or 5 mice per group (in case of WM3918). Statistical significance was determined by two-way ANOVA.

Figure 2. MTX-216 co-suppresses Ki-67 and p-S6 and induces apoptosis in NF1^{LoF} cells. (a, b) MTX-216 dose-dependent changes in apoptotic response of COLO792 cells (after 48 h) and WM3918 and MeWo cells (after 72 h), measured using a NucView Caspase-3 reporter assay. Single-cell NucView intensities across different inhibitor doses **(a)** and the estimation of the percentage of apoptotic cells based on NucView intensity gating **(b)** are shown for each cell line. Data are presented as mean values ± s.d. calculated across n = 2 replicates. **(c)** Two-sided Pearson's correlation analysis between the percentage of p-S6$^{Low/}$Ki-67^{Low} cells and the inhibitor-induced normalized growth rate (measured after 72 h of treatment) across three NF1^{LoF}/BRAF^{WT} melanoma cell lines (MeWo, WM3918 and COLO792) and one NF1^{WT}/BRAF^{V600E} cell line (COLO858) treated with MTX-216, trametinib, ulixertinib and pictilisib (at the same concentrations as shown in Fig. 1b). **(d)** Co-variate single-cell analysis of p-S6 versus Ki-67 across three NF1^{LoF}/BRAF^{WT} melanoma cell lines (MeWo, WM3918 and COLO792) and one NF1^{WT}/BRAF^{V600E} cell line (COLO858) treated for 72 h with indicated concentrations of MTX-216, trametinib, ulixertinib and pictilisib. The horizontal and vertical dash lines were used to gate Ki-67^{High} versus Ki-67^{Low} cells and p-S6^{High} versus p-S6^{Low} cells, respectively. Percentages of cells in each quadrant are shown in red.

Figure 3. SYK kinase activity is more effectively inhibited by MTX-216 than by MTX-211. (a) High-throughput kinase inhibition assays (using Z'-LYTE and Adapta platforms) reporting % inhibition of 403 kinases by MTX-216 and MTX-211 (both at 10 μM) in the presence of ATP at a concentration of $K_{m,app}$ for each target. Dashed line represents $y = x$. **(b)** Half-maximal inhibitory concentration (IC_{50}) values for the nominal targets of MTX-216 and MTX-211 (PI3K and EGFR) as well as other kinases that were inhibited significantly (>90%) by both compounds (at 10 μM). IC_{50} values were derived from kinase activity assays performed across 10 concentrations (using 3-fold serial dilutions) of each compound. Dashed line represents $y = x$. **(c)** Dose-dependent inhibition of SYK kinase activity by MTX-216 and MTX-211. Data are presented as mean values ± s.d. calculated across n = 2 replicates. **(d, e)** Western blot measurements **(d)** and their quantification **(e)** for p-$SYK^{Y525/526}$ relative to total SYK in MeWo cells treated for 24 h with indicated concentrations of MTX-216, MTX-211, R406 and entospletinib. Data across different treatments conditions are normalized to DMSO-treated cells. **(f)** Differentially up- or down-regulated genes by MTX-216 and MTX-211 (relative to DMSO) following 24 h treatment of WM3918 and MeWo cells. Significant genes were identified as $|\log_2(\text{fold change})| \geq 1$ and adjusted P value (FDR) ≤ 0.05. See also Supplementary Dataset 1. **(g)** Number of significant genes up- or down-regulated by only one of the compounds or by both compounds in each of the WM3918 and MeWo cell lines. **(h)** Number of genes down-regulated specifically by MTX-216 in either or both of WM3918 and MeWo cell lines. **(i)** Top enriched kinase perturbation terms associated with 231 genes down-regulated specifically by MTX-216 (but not by MTX-211) in both WM3918 and MeWo cell lines. See also Supplementary Dataset 2.

Figure 4. SYK inhibition or depletion reduces the growth of $NF1^{LoF}$ melanoma cells and increases their sensitivity to both PI3K and MEK inhibitors. (a) SYK protein levels assessed by Western blots

in MeWo (top) and YUHEF cells (bottom) following treatment with pooled siRNAs targeting SYK isoforms or with non-targeting (control) siRNA for 72 h. Each siRNA experiment was performed in two independent replicates. **(b)** Normalized growth rates measured in MeWo (top) and YUHEF cells (bottom) following 72 h treatment with indicated concentrations of MTX-211, trametinib, or pictilisib (all dissolved in DMSO as vehicle) in the presence of pooled siRNAs targeting SYK or non-targeting (control) siRNA (for 72 h). Data are presented as mean values ± s.d. calculated across n = 3 replicates. Statistical significance of the effect of SYK siRNA (versus control siRNA) in the absence of all inhibitors was determined by two-sided, two-sample *t*-test. Statistical significance of the effect of SYK siRNA (versus control siRNA) in the presence of inhibitors at three indicated concentrations was determined by two-way ANOVA. **(c)** Normalized growth rates measured in MeWo (top) and YUHEF cells (bottom) following 7-day treatments with indicated concentrations of MTX-211, trametinib, or pictilisib (all dissolved in DMSO as vehicle) in combination with either R406 (at 3.16 μM) or vehicle (DMSO). Data are presented as mean values ± s.d. calculated across n = 2 replicates. Statistical significance of the effect of R406 (versus DMSO) in the absence of other inhibitors was determined by two-sided, two-sample *t*-test. Statistical significance of the effect of R406 (versus DMSO) in the presence of other inhibitors at four indicated concentrations was determined by two-way ANOVA.

Figure 5. MTX-216 suppresses mitochondrial electron transport chain genes in NF1^{LoF} cells. (a-c) Principal component analysis of gene expression variations across 42 samples, representing 3 cell lines (MeWo, WM3918 and SKMEL113) and 24 h treatment conditions with MTX-216 (at 1 μM), MTX-211 (at 1 μM), pictilisib (at 1 μM), trametinib (at 0.1 μM), the combination of MTX-216 (at 1 μM) and trametinib (at 0.1 μM), or DMSO, each tested in 3 independent replicates. See also Supplementary Dataset 3. **(a)** Percentage of variance captured by the first five principal components (PCs). **(b)** PC3 and

PC4 scores, capturing treatment-specific variations in gene expression across the samples. Arrows show changes of scores (in PC3-PC4 space) by specific treatments relative to DMSO-treated cells. **(c)** PC3 and PC4 loadings, highlighting genes associated with distinct inhibitory effects on $NF1^{LoF}$ cells. Gene loadings differentially enriched along either PC3 or PC4 based on a ratio cutoff of *cotangent* ($\pi/8$) ≈ 2.4 and with loading values of greater than 1.5×median (for positive loadings) or smaller than 1.5×median (for negative loadings) are highlighted in color. See also Supplementary Dataset 4. **(d)** The top Gene Ontology (GO) terms with FDR ≤ 0.05 associated with significantly negative PC3 and significantly negative PC4 loadings. See also Supplementary Dataset 5. **(e)** Gene set enrichment analysis (GSEA) of genes down-regulated by MTX-216 in three cell lines (MeWo, WM3918 and SKMEL113) using consolidated Hallmark gene sets. Hallmark terms with FDR ≤ 0.05 in all three cell lines are highlighted in red. See also Supplementary Datasets 6, 7. **(f)** DMSO-normalized gene expression (transcripts per million; TPM) levels of electron transport chain genes NDUFA1, NDUFB1, UQCRQ and COX5A in three cell lines following 24 h treatment with MTX-216 and trametinib. Data are presented as mean values ± s.d. calculated across n = 3 replicates. Statistical significance was determined by two-way ANOVA.

Figure 6. Mitochondrial respiratory chain is associated with poor survival in $NF1^{LoF}$ melanomas patients and inhibitable by MTX-216 or SYK inhibition. (a-c) Overall survival of NF1-, BRAF-, and NRAS-mutated patients from The Cancer Genome Atlas (TCGA) melanoma cohort classified into two groups with high (ETC^{High}) and low (ETC^{Low}) respiratory electron transport chain gene signature. Statistical significance was determined by two-sided log-rank (Mantel-Cox) test and corrected using the Benjamini-Hochberg FDR procedure. **(d)** Log-normalized changes in live cell count following the exposure of two cell lines MeWo and WM3918 to indicated doses of IACS-010759 for a period of 13

and 7 days, respectively. Data are presented as mean values ± s.d. calculated across n = 2 replicates. **(e, f)** Changes in mitochondrial mass measured by MitoTracker Deep Red **(e)**, and mitochondrial membrane potential measured by MitoTracker Red CMXRos **(f)**, in MeWo cells in the presence of pooled SYK siRNAs or nontargeting (control) siRNA for 72 h. Single-cell intensities (left) and the population-averaged data (right) are shown for each measurement. Population-averaged data are presented as mean values ± s.d. calculated across n = 3 replicates. Statistical significance was determined by two-sided, two-sample *t*-test. **(g, h)** Changes in mitochondrial mass measured by MitoTracker Deep Red **(g)**, and mitochondrial membrane potential measured by MitoTracker Red CMXRos **(h)**, in MeWo and WM3918 cells following 48 h treatment with MTX-216 (at 1 μM) or DMSO. Single-cell intensities (left) and the population-averaged data (right) are shown for each measurement. Population-averaged data are presented as mean values ± s.d. calculated across n = 3 replicates. Statistical significance was determined by two-sided, two-sample *t*-test.

Supplementary Figure Legends

Supplementary Figure 1. A targeted compound screen identifies MTX-216 as an efficacious inhibitor of NF1^{LoF} melanoma cells. a) The chemical structure of MTX-216 (N-(2-chloro-5-(4-((3-chloro-4-fluorophenyl)amino)-3-cyanoquinolin-6-yl)pyridin-3-yl)methanesulfonamide). Also included in this study was MTX-211 (N-(2-chloro-5-(4-((3-chloro-4-fluorophenyl)amino)quinazolin-6-yl)pyridin-3-yl)methanesulfonamide), a closely related structural analog of MTX-216. **(b)** List of cell lines used in this study and their NF1, BRAF, and NRAS mutation status. **(c)** Dose-dependent changes in normalized growth rates (a.k.a. DIP rates) calculated by dividing the 7-day average net growth rate for inhibitor-treated cells to that measured for vehicle (DMSO)-treated cells across cell lines with different NF1/BRAF/NRAS mutation status. The average net growth rates for each condition were calculated

from measurements of live cell count (across two replicates) at four timepoints (including 1, 3, 5, and 7 days). Normalized growth rates < 0 indicate a net cell loss (i.e., inhibitor-induced cytotoxicity), a value of 0 represent no change in viable cell number (i.e., cytostasis), a value > 0 indicates a net cell gain, and a value of 1 represents no effect as cells grow in the presence of inhibitor at the same rate as in the DMSO condition. For combination, the concentration of one inhibitor was varied between 0 and the indicated C_{max} value in the presence of a fixed concentration of a second inhibitor. **(d)** Body weight change in mice implanted subcutaneously with WM3918 and COLO792 tumor cells following intraperitoneal (IP) treatments with MTX-216 or vehicle in two different dosing regimens as described in Methods. Data represent mean values ± s.e.m across 4 mice per group (in case of COLO792) or 5 mice per group (in case of WM3918).

Supplementary Figure 2. MTX-216 co-suppresses Ki-67 and p-S6 in NF1^{LoF} cells. Representative multiplexed immunofluorescent images of Ki-67 and phosphorylated S6 ribosomal protein (p-S6$^{S235/S236}$), co-stained in MeWo cells following 72 h treatment with indicated concentrations of trametinib, pictilisib, MTX-216 or DMSO. Each experiment was repeated twice independently with similar results. Scale bars represent 100 µm.

Supplementary Figure 3. Kinase inhibition assays and differential gene expression analysis of MTX-216 and MTX-211. (a) Dose-dependent inhibition of kinase activities by MTX-216 and MTX-211. Data are presented as mean values ± s.d. calculated across n = 2 replicates. Kinase inhibition assays (using Z'-LYTE and Adapta platforms) were performed in the presence of ATP at a concentration of $K_{m,app}$ for each target. **(b)** Number of genes up-regulated specifically by MTX-216 in either or both of WM3918 and MeWo cell lines. **(c)** Top enriched kinase perturbation terms associated with 467 genes

up-regulated specifically by MTX-216 (but not by MTX-211) in both WM3918 and MeWo cell lines.

Supplementary Figure 4. SYK inhibition reduces the growth of WM3918 cells and increases their sensitivity to MTX-211 and trametinib. Normalized growth rates measured in WM3918 cells following 7-day treatments with indicated concentrations of MTX-211 or trametinib (both dissolved in DMSO as vehicle) in combination with either R406 (at 3.16 μM) or vehicle (DMSO). Data are presented as mean values ± s.d. calculated across n = 2 replicates. Statistical significance of the effect of R406 (versus DMSO) in the absence of the other inhibitors was determined by two-sided, two-sample t-test. Statistical significance of the effect of R406 (versus DMSO) in the presence of other inhibitors at four indicated concentrations was determined by two-way ANOVA.

Supplementary Figure 5. Statistical and bioinformatics analyses identify genes differentially enriched by trametinib versus MTX-216 in NF1^{LoF} cells. (a) Principal component analysis of gene expression variations across 42 samples, representing 3 cell lines (MeWo, WM3918 and SKMEL113) and 24 h treatment conditions with MTX-216 (at 1 μM), MTX-211 (at 1 μM), pictilisib (at 1 μM), trametinib (at 0.1 μM), the combination of MTX-216 (at 1 μM) and trametinib (at 0.1 μM), or DMSO, each tested in 3 independent replicates. PC1 and PC2 scores capture cell line-specific variations, while PC3 and PC4 scores capture inhibitor-specific variations in gene expression across the samples. **(b)** Hierarchical clustering of $\log_2$ fold changes (relative to DMSO) in the expression of genes with significantly negative PC4 loadings (top) or genes with significantly negative PC3 loadings (bottom) following treatment with indicated inhibitors. **(c**) Gene set enrichment analysis (GSEA) of genes down-regulated by trametinib in three cell lines (MeWo, WM3918 and SKMEL113) using consolidated Hallmark gene sets. Hallmark terms with FDR ≤ 0.05 in all three cell lines are highlighted in red.

Supplementary Figure 6. Mitochondrial respiratory chain is associated with poor survival in $NF1^{LoF}$ melanomas patients and inhibitable by MTX-216. (a) Distribution of summed z-scores for respiratory electron transport chain (ETC) genes across 339 TCGA melanoma patient samples. Dashed line (z = 0) represents threshold to identify tumors that are high or low in expression of 116 ETC genes. Positive summed scores are tumors enriched in ETC signature (i.e., ETC^{High}) and negative summed scores represent tumors that are low in ETC signature (i.e., ETC^{Low}). **(b)** Representative multiplexed fluorescent images of MitoTracker Deep Red and MitoTracker CMXRos, co-stained in WM3918 cells following 48 h treatment with indicated concentration of MTX-216 or DMSO. Each experiment was repeated three times independently with similar results. Scale bars represent 100 µm.

Supplementary Datasets

Supplementary Dataset 1. Differential gene expression analysis performed on MeWo and WM3918 cells treated with either MTX-216 (1 µM) or MTX-211 (1 µM) relative to DMSO for 24 h.

Supplementary Dataset 2. Enriched Gene Ontology Omnibus (GEO) kinase perturbation terms associated with genes downregulated or upregulated specifically by MTX-216 (but not by MTX-211) in both WM3918 and MeWo cell lines.

Supplementary Dataset 3. Quantified gene expression data (TPM) from RNA sequencing analysis of MeWo, WM3918 or SKMEL113 cells treated with indicated compounds and concentrations, or vehicle (DMSO) for 24 h in three replicates.

Supplementary Dataset 4. Principal Component Analysis (PCA) scores and associated gene loadings following the analysis of data across 42 samples, representing different treatment conditions, cell lines and replicates.

Supplementary Dataset 5. The top Gene Ontology (GO) terms associated with significantly negative or positive PC3 or PC4 loadings.

Supplementary Dataset 6. Differential gene expression analysis performed on MeWo and WM3918 cells treated with Trametinib (0.1 µM) for 24 h and SKMEL113 cells treated with either MTX-216 (1 µM) or Trametinib (0.1 µM) relative to DMSO for 24 h.

Supplementary Dataset 7. Gene set enrichment analysis (GSEA) of genes down-regulated by MTX-216 or trametinib (relative to DMSO) in three cell lines (MeWo, WM3918 and SKMEL113) using consolidated Hallmark gene sets.

References

1. Cancer Genome Atlas Network. Genomic Classification of Cutaneous Melanoma. *Cell* **161**, 1681–1696 (2015).
2. Bollag, G. *et al.* Vemurafenib: the first drug approved for BRAF-mutant cancer. *Nat Rev Drug Discov* **11**, 873–886 (2012).
3. Krauthammer, M. *et al.* Exome sequencing identifies recurrent mutations in NF1 and RASopathy genes in sun-exposed melanomas. *Nat Genet* **47**, 996–1002 (2015).

4. Sullivan, R. J. The role of mitogen-activated protein targeting in melanoma beyond BRAFV600. *Curr Opin Oncol* **28**, 185–191 (2016).
5. Hayward, N. K. *et al.* Whole-genome landscapes of major melanoma subtypes. *Nature* **545**, 175–180 (2017).
6. Maertens, O. *et al.* Elucidating Distinct Roles for NF1 in Melanomagenesis. *Cancer Discov* **3**, 338–349 (2013).
7. Nissan, M. H. *et al.* Loss of NF1 in Cutaneous Melanoma Is Associated with RAS Activation and MEK Dependence. *Cancer Res* **74**, 2340–2350 (2014).
8. Ranzani, M. *et al.* BRAF/NRAS wild-type melanoma, NF1 status and sensitivity to trametinib. *Pigment Cell Melanoma Res* **28**, 117–119 (2015).
9. Lock, R. *et al.* Cotargeting MNK and MEK kinases induces the regression of NF1-mutant cancers. *J Clin Invest* **126**, 2181–2190 (2016).
10. Malone, C. F. *et al.* mTOR and HDAC Inhibitors Converge on the TXNIP/Thioredoxin Pathway to Cause Catastrophic Oxidative Stress and Regression of RAS-Driven Tumors. *Cancer Discov* **7**, 1450–1463 (2017).
11. Trousil, S. *et al.* Phenformin Enhances the Efficacy of ERK Inhibition in NF1-Mutant Melanoma. *J Invest Dermatol* **137**, 1135–1143 (2017).
12. Malone, C. F. *et al.* Defining key signaling nodes and therapeutic biomarkers in NF1-mutant cancers. *Cancer Discov* **4**, 1062–1073 (2014).
13. Nichols, R. J. *et al.* RAS nucleotide cycling underlies the SHP2 phosphatase dependence of mutant BRAF-, NF1- and RAS-driven cancers. *Nat Cell Biol* **20**, 1064–1073 (2018).
14. Garuti, L., Roberti, M. & Bottegoni, G. Multi-kinase inhibitors. *Curr Med Chem* **22**, 695–712 (2015).

15. Knight, Z. A., Lin, H. & Shokat, K. M. Targeting the cancer kinome through polypharmacology. *Nat Rev Cancer* **10**, 130–137 (2010).

16. Patterson, H. C. *et al.* A respiratory chain controlled signal transduction cascade in the mitochondrial intermembrane space mediates hydrogen peroxide signaling. *Proc Natl Acad Sci U S A* **112**, E5679-5688 (2015).

17. Molina, J. R. *et al.* An inhibitor of oxidative phosphorylation exploits cancer vulnerability. *Nat Med* **24**, 1036–1046 (2018).

18. Harris, L. A. *et al.* An unbiased metric of antiproliferative drug effect in vitro. *Nat Methods* **13**, 497–500 (2016).

19. Fallahi-Sichani, M. *et al.* Systematic analysis of BRAF(V600E) melanomas reveals a role for JNK/c-Jun pathway in adaptive resistance to drug-induced apoptosis. *Mol Syst Biol* **11**, 797 (2015).

20. Magnuson, B., Ekim, B. & Fingar, D. C. Regulation and function of ribosomal protein S6 kinase (S6K) within mTOR signalling networks. *Biochem J* **441**, 1–21 (2012).

21. Roux, P. P. *et al.* RAS/ERK Signaling Promotes Site-specific Ribosomal Protein S6 Phosphorylation via RSK and Stimulates Cap-dependent Translation. *J Biol Chem* **282**, 14056–14064 (2007).

22. Romeo, Y., Zhang, X. & Roux, P. P. Regulation and function of the RSK family of protein kinases. *Biochem J* **441**, 553–569 (2012).

23. Miller, I. *et al.* Ki67 is a Graded Rather than a Binary Marker of Proliferation versus Quiescence. *Cell Rep* **24**, 1105-1112.e5 (2018).

24. Jabril-Cuenod, B. *et al.* Syk-dependent phosphorylation of Shc. A potential link between FcepsilonRI and the Ras/mitogen-activated protein kinase signaling pathway through SOS and Grb2. *J Biol Chem* **271**, 16268–16272 (1996).

25. Kawakami, Y. *et al.* A Ras activation pathway dependent on Syk phosphorylation of protein kinase C. *Proc Natl Acad Sci U S A* **100**, 9470–9475 (2003).

26. Furlong, M. T. *et al.* Identification of the major sites of autophosphorylation of the murine protein-tyrosine kinase Syk. *Biochim Biophys Acta* **1355**, 177–190 (1997).

27. Cremer, A. *et al.* Resistance Mechanisms to SYK Inhibition in Acute Myeloid Leukemia. *Cancer Discov* **10**, 214–231 (2020).

28. Walker, A. R. *et al.* Interim Results of a Phase 1b/2 Study of Entospletinib (GS-9973) Monotherapy and in Combination with Chemotherapy in Patients with Acute Myeloid Leukemia. *Blood* **128**, 2831 (2016).

29. Braselmann, S. *et al.* R406, an Orally Available Spleen Tyrosine Kinase Inhibitor Blocks Fc Receptor Signaling and Reduces Immune Complex-Mediated Inflammation. *J Pharmacol Exp Ther* **319**, 998–1008 (2006).

30. Kuleshov, M. V. *et al.* Enrichr: a comprehensive gene set enrichment analysis web server 2016 update. *Nucleic Acids Res* **44**, W90–W97 (2016).

31. Liberzon, A. *et al.* The Molecular Signatures Database (MSigDB) hallmark gene set collection. *Cell Syst* **1**, 417–425 (2015).

32. Valle, S. *et al.* Exploiting oxidative phosphorylation to promote the stem and immunoevasive properties of pancreatic cancer stem cells. *Nat Commun* **11**, 5265 (2020).

33. Lito, P. *et al.* Relief of profound feedback inhibition of mitogenic signaling by RAF inhibitors attenuates their activity in BRAFV600E melanomas. *Cancer Cell* **22**, 668–682 (2012).

34. Mócsai, A., Ruland, J. & Tybulewicz, V. L. J. The SYK tyrosine kinase: a crucial player in diverse biological functions. *Nat Rev Immunol* **10**, 387–402 (2010).

35. Larive, R. M. *et al.* Phosphoproteomic analysis of Syk kinase signaling in human cancer cells reveals its role in cell-cell adhesion. *Oncogene* **28**, 2337–2347 (2009).

36. Zhang, X., Shrikhande, U., Alicie, B. M., Zhou, Q. & Geahlen, R. L. Role of the protein tyrosine kinase Syk in regulating cell-cell adhesion and motility in breast cancer cells. *Mol Cancer Res* **7**, 634–644 (2009).

37. Polak, A. *et al.* SYK inhibition targets acute myeloid leukemia stem cells by blocking their oxidative metabolism. *Cell Death Dis* **11**, 956 (2020).

38. Chen, L. *et al.* SYK Inhibition Modulates Distinct PI3K/AKT- Dependent Survival Pathways and Cholesterol Biosynthesis in Diffuse Large B Cell Lymphomas. *Cancer Cell* **23**, 826–838 (2013).

39. Caro, P. *et al.* Metabolic signatures uncover distinct targets in molecular subsets of diffuse large B cell lymphoma. *Cancer Cell* **22**, 547–560 (2012).

40. Chopra, S. S. *et al.* Torin2 Exploits Replication and Checkpoint Vulnerabilities to Cause Death of PI3K-Activated Triple-Negative Breast Cancer Cells. *Cell Syst* **10**, 66-81.e11 (2020).

41. Jeong, W., Doroshow, J. H. & Kummar, S. United States Food and Drug Administration approved oral kinase inhibitors for the treatment of malignancies. *Curr Probl Cancer* **37**, 110–144 (2013).

42. Lin, A. *et al.* Off-target toxicity is a common mechanism of action of cancer drugs undergoing clinical trials. *Sci Transl Med* **11**, (2019).

43. Hafner, M. *et al.* Multiomics Profiling Establishes the Polypharmacology of FDA-Approved CDK4/6 Inhibitors and the Potential for Differential Clinical Activity. *Cell Chem Biol* **26**, 1067-1080.e8 (2019).

44. McQuin, C. *et al.* CellProfiler 3.0: Next-generation image processing for biology. *PLoS Biol* **16**, e2005970 (2018).

45. Kim, D., Paggi, J. M., Park, C., Bennett, C. & Salzberg, S. L. Graph-based genome alignment and genotyping with HISAT2 and HISAT-genotype. *Nature Biotechnology* **37**, 907–915 (2019).

46. Pertea, M. *et al.* StringTie enables improved reconstruction of a transcriptome from RNA-seq reads. *Nature Biotechnology* **33**, 290–295 (2015).

47. Pertea, M., Kim, D., Pertea, G. M., Leek, J. T. & Salzberg, S. L. Transcript-level expression analysis of RNA-seq experiments with HISAT, StringTie and Ballgown. *Nature Protocols* **11**, 1650–1667 (2016).

48. Love, M. I., Huber, W. & Anders, S. Moderated estimation of fold change and dispersion for RNA-seq data with DESeq2. *Genome Biology* **15**, 550 (2014).

49. Afgan, E. *et al.* The Galaxy platform for accessible, reproducible and collaborative biomedical analyses: 2018 update. *Nucleic Acids Res* **46**, W537–W544 (2018).

50. Wang, Z. *et al.* Extraction and analysis of signatures from the Gene Expression Omnibus by the crowd. *Nature Communications* **7**, 12846 (2016).

51. Subramanian, A. *et al.* Gene set enrichment analysis: A knowledge-based approach for interpreting genome-wide expression profiles. *Proc Natl Acad Sci USA* **102**, 15545 (2005).

52. Mootha, V. K. *et al.* PGC-1α-responsive genes involved in oxidative phosphorylation are coordinately downregulated in human diabetes. *Nature Genetics* **34**, 267–273 (2003).

53. Cerami, E. *et al.* The cBio cancer genomics portal: an open platform for exploring multidimensional cancer genomics data. *Cancer Discov* **2**, 401–404 (2012).

Figure 1

a

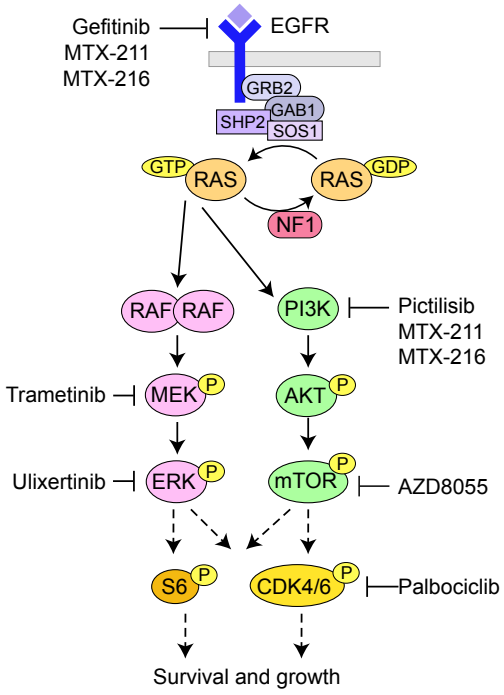

b

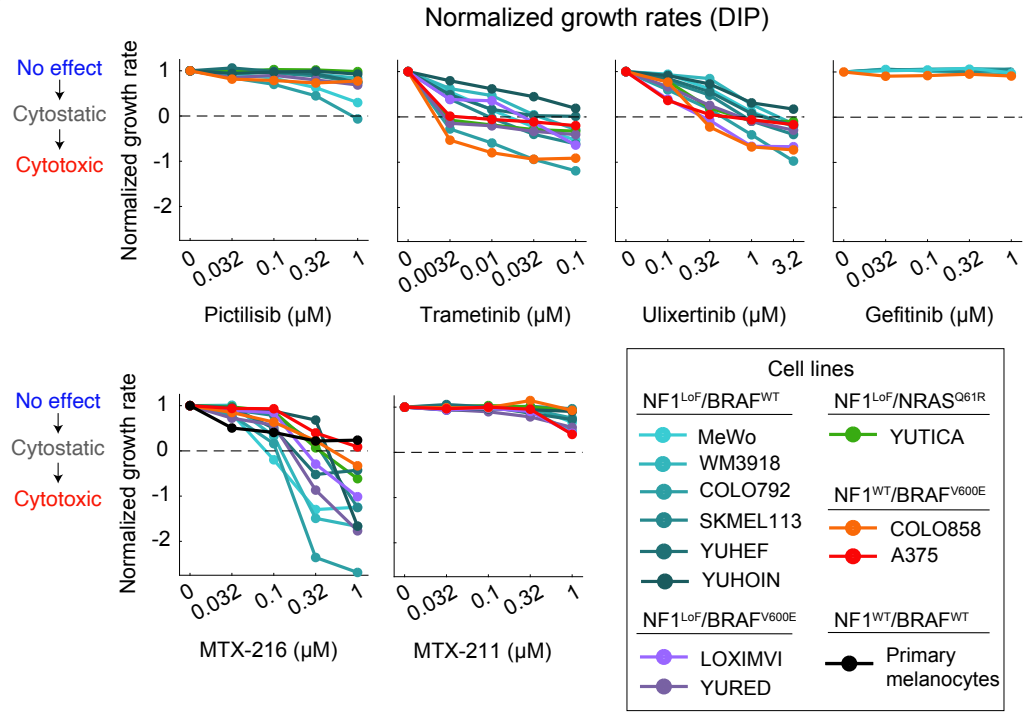

c

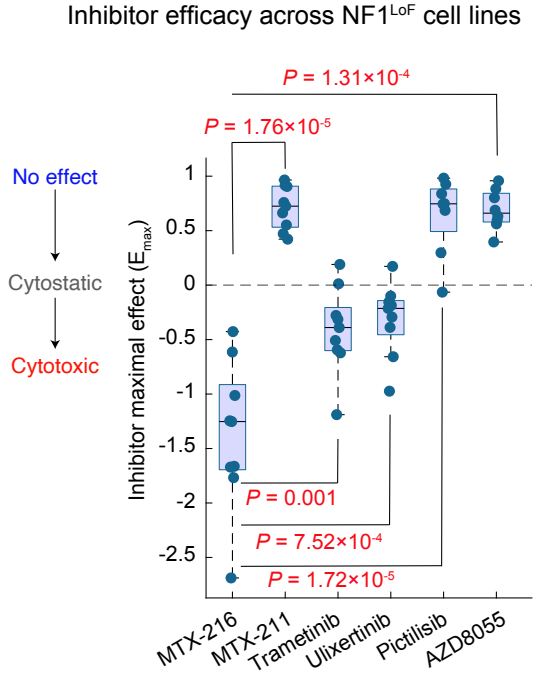

d

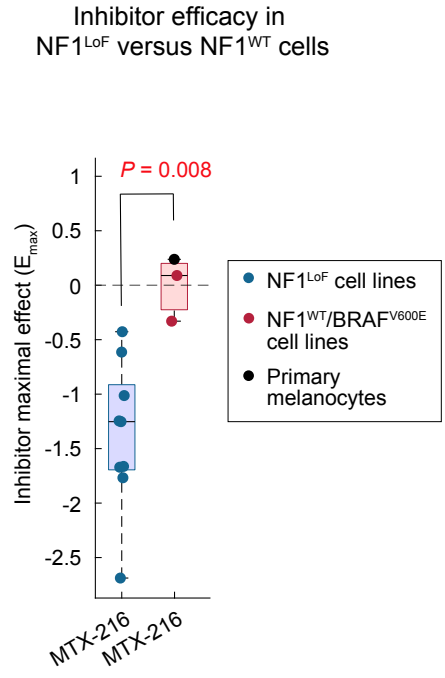

e

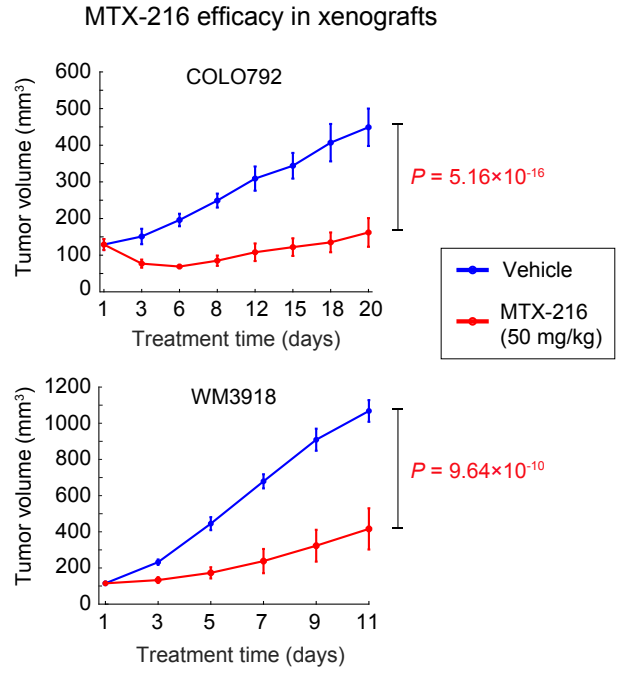

Figure 2

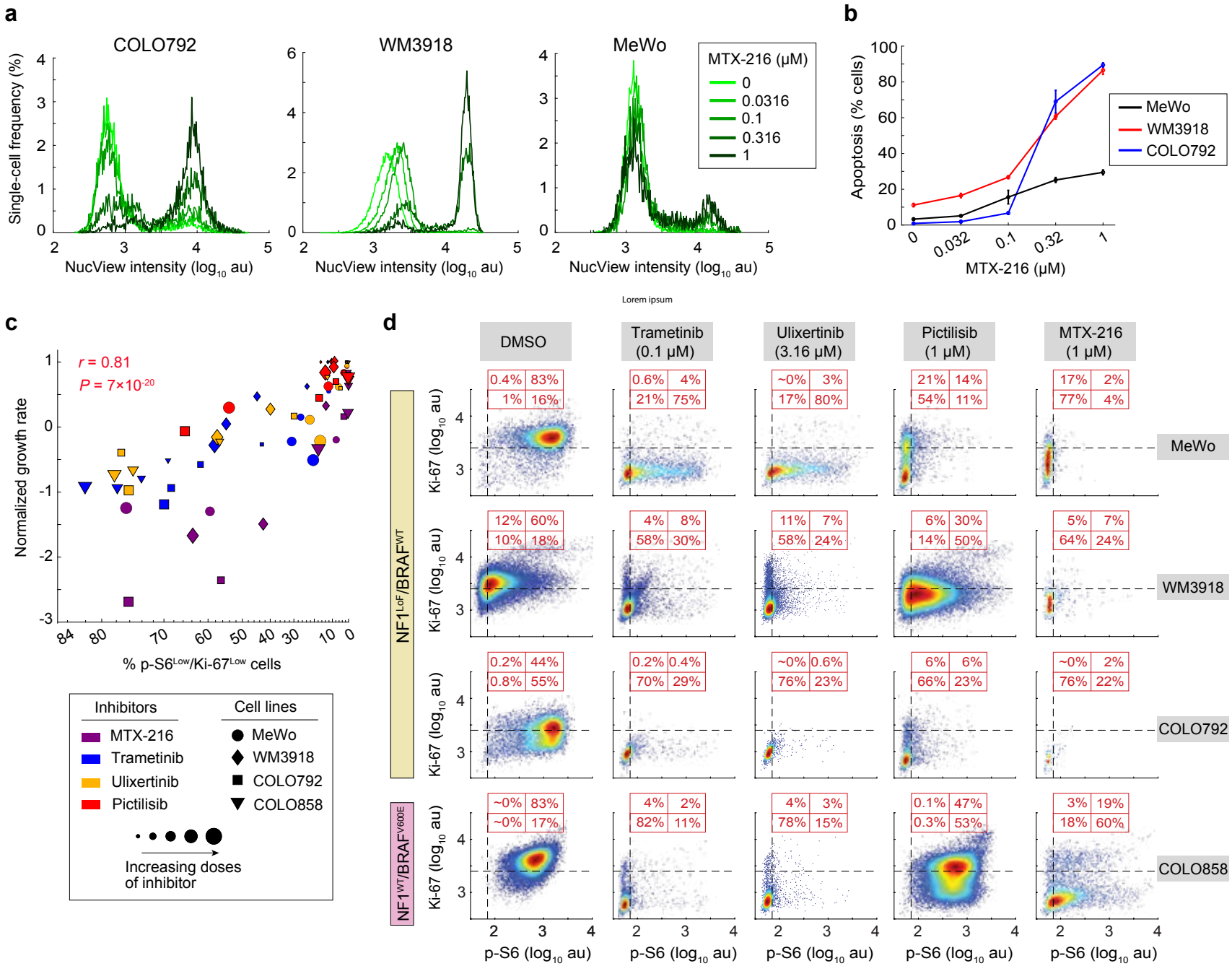
a
COLO792
WM3918
MeWo
Single-cell frequency (%)
NucView intensity (log10 au)
MTX-216 (μM)
0
0.0316
0.1
0.316
1
b
Apoptosis (% cells)
MTX-216 (μM)
MeWo
WM3918
COLO792
Lorem ipsum
c
r = 0.81
P = 7×10-20
Normalized growth rate
% p-S6Low/Ki-67Low cells
Inhibitors
MTX-216
Trametinib
Ulixertinib
Pictilisib
Cell lines
MeWo
WM3918
COLO792
COLO858
Increasing doses of inhibitor
d
DMSO
Trametinib (0.1 μM)
Ulixertinib (3.16 μM)
Pictilisib (1 μM)
MTX-216 (1 μM)
NF1LOF/BRAFWT
NF1WT/BRAFV600E
Ki-67 (log10 au)
p-S6 (log10 au)
MeWo
WM3918
COLO792
COLO858

Figure 3

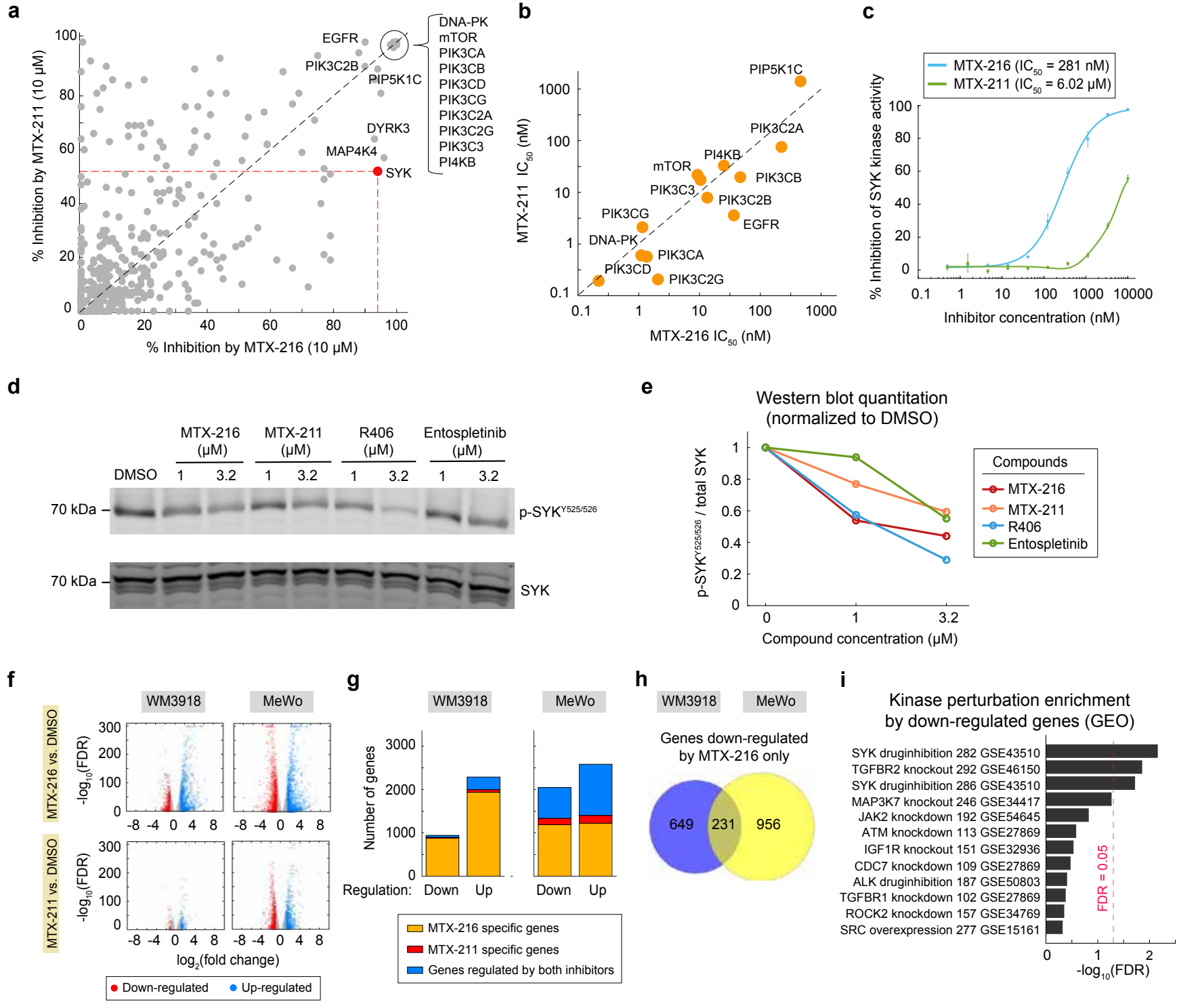
a
% Inhibition by MTX-211 (10 μM)
% Inhibition by MTX-216 (10 μM)
EGFR
PIK3C2B
PIP5K1C
DYRK3
MAP4K4
SYK
DNA-PK
mTOR
PIK3CA
PIK3CB
PIK3CD
PIK3CG
PIK3C2A
PIK3C2G
PIK3C3
PI4KB
b
MTX-211 IC50 (nM)
MTX-216 IC50 (nM)
PIP5K1C
PIK3C2A
PI4KB
mTOR
PIK3CB
PIK3C3
PIK3C2B
EGFR
PIK3CG
DNA-PK
PIK3CA
PIK3CD
PIK3C2G
c
MTX-216 (IC50 = 281 nM)
MTX-211 (IC50 = 6.02 μM)
% Inhibition of SYK kinase activity
Inhibitor concentration (nM)
d
MTX-216 (μM)
MTX-211 (μM)
R406 (μM)
Entospletinib (μM)
DMSO
1
3.2
70 kDa
p-SYKY525/526
SYK
e
Western blot quantitation (normalized to DMSO)
p-SYKY525/526 / total SYK
Compound concentration (μM)
Compounds
MTX-216
MTX-211
R406
Entospletinib
f
WM3918
MeWo
MTX-216 vs. DMSO
MTX-211 vs. DMSO
-log10(FDR)
log2(fold change)
Down-regulated
Up-regulated
g
WM3918
MeWo
Number of genes
Regulation: Down Up
MTX-216 specific genes
MTX-211 specific genes
Genes regulated by both inhibitors
h
WM3918
MeWo
Genes down-regulated by MTX-216 only
649
231
956
i
Kinase perturbation enrichment by down-regulated genes (GEO)
SYK druginhibition 282 GSE43510
TGFBR2 knockout 292 GSE46150
SYK druginhibition 286 GSE43510
MAP3K7 knockout 246 GSE34417
JAK2 knockdown 192 GSE54645
ATM knockdown 113 GSE27869
IGF1R knockout 151 GSE32936
CDC7 knockdown 109 GSE27869
ALK druginhibition 187 GSE50803
TGFBR1 knockdown 102 GSE27869
ROCK2 knockdown 157 GSE34769
SRC overexpression 277 GSE15161
FDR = 0.05
-log10(FDR)

Figure 4

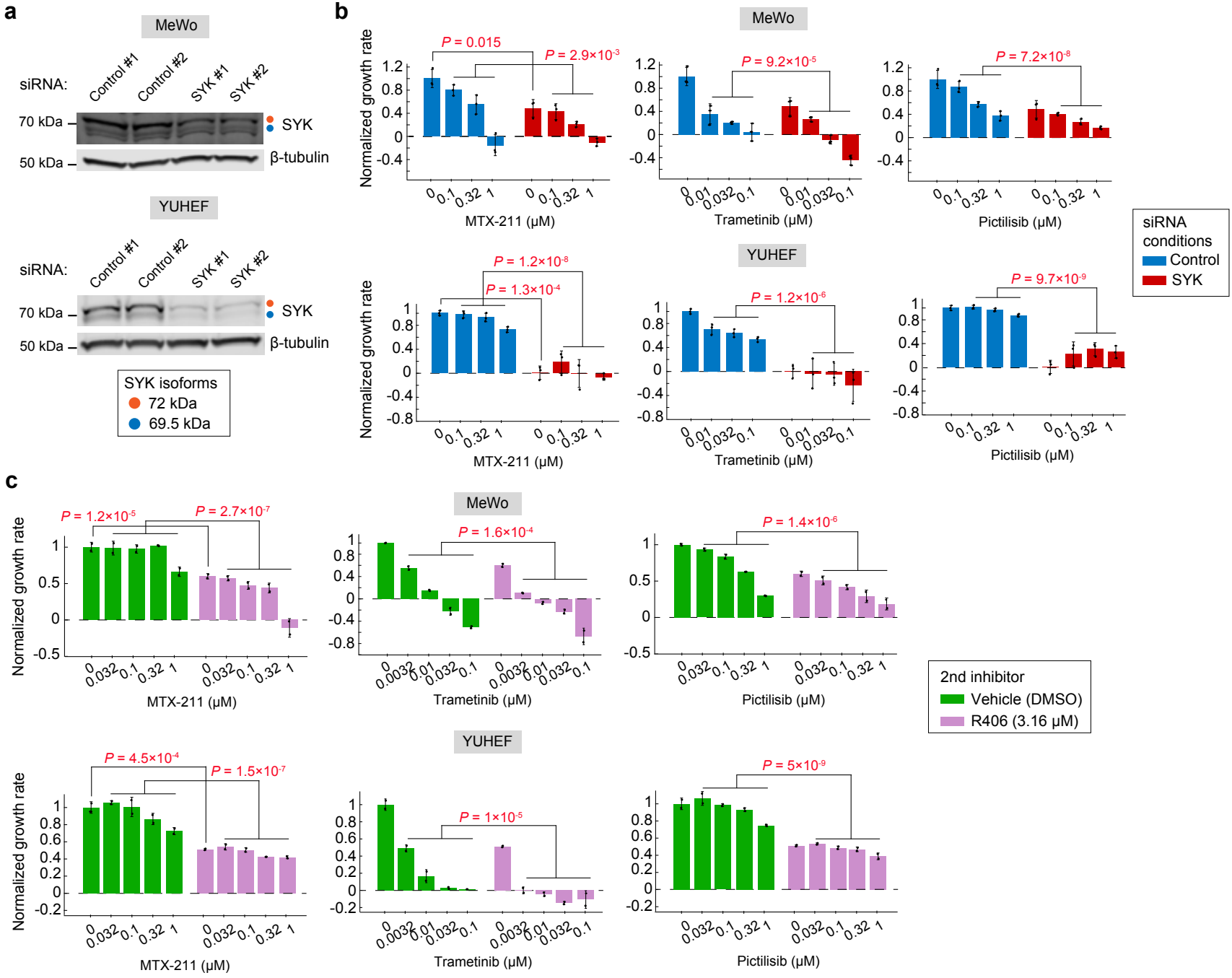
a
MeWo
siRNA:
Control #1
Control #2
SYK #1
SYK #2
70 kDa
50 kDa
SYK
β-tubulin
YUHEF
SYK isoforms
72 kDa
69.5 kDa
b
Normalized growth rate
P = 0.015
P = 2.9×10-3
P = 9.2×10-5
P = 7.2×10-8
P = 1.2×10-8
P = 1.3×10-4
P = 1.2×10-6
P = 9.7×10-9
MTX-211 (μM)
Trametinib (μM)
Pictilisib (μM)
siRNA conditions
Control
SYK
c
P = 1.2×10-5
P = 2.7×10-7
P = 1.6×10-4
P = 1.4×10-6
P = 4.5×10-4
P = 1.5×10-7
P = 1×10-5
P = 5×10-9
2nd inhibitor
Vehicle (DMSO)
R406 (3.16 μM)

Figure 5

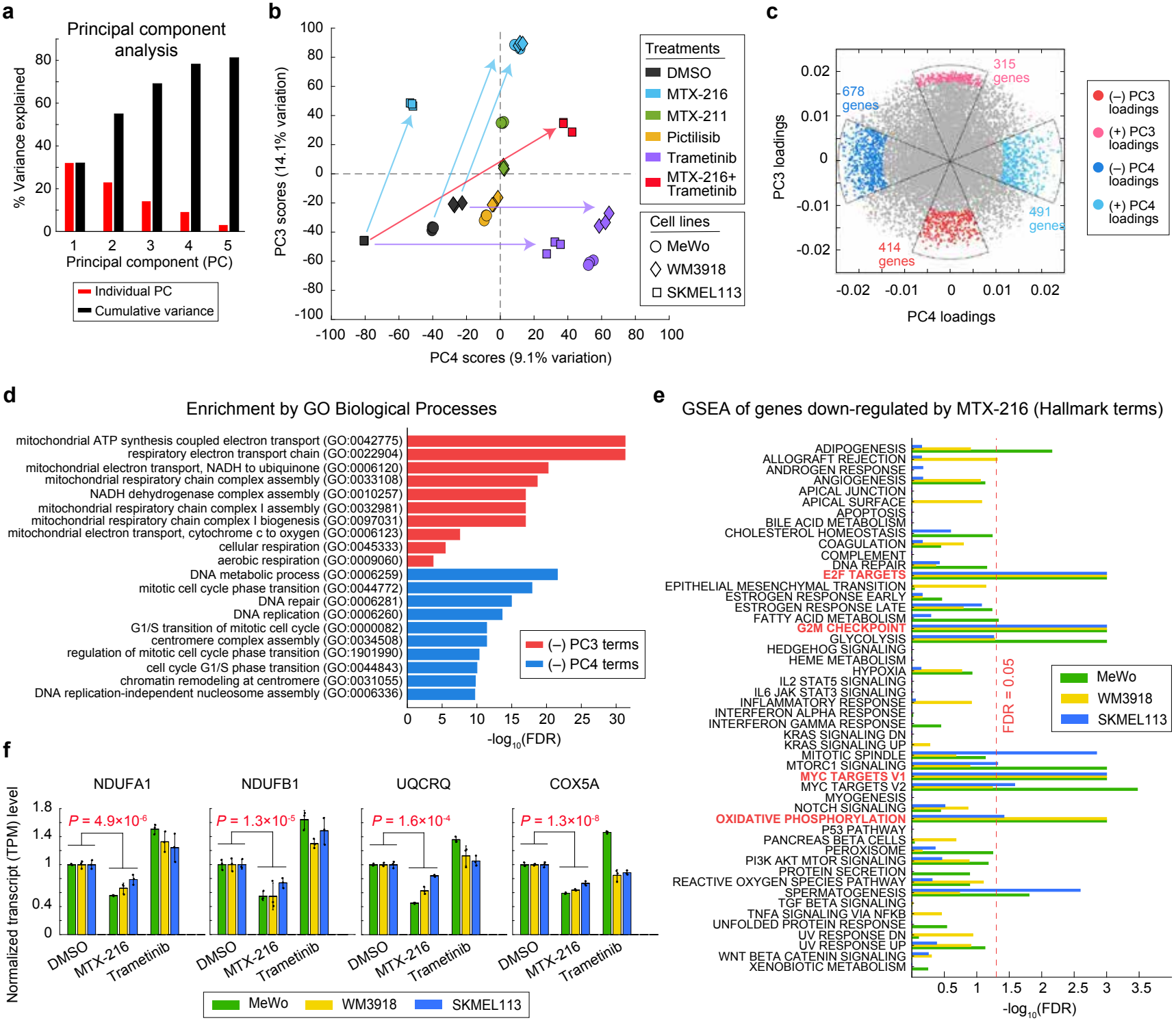
a
Principal component analysis
% Variance explained
Principal component (PC)
Individual PC
Cumulative variance
b
PC3 scores (14.1% variation)
PC4 scores (9.1% variation)
Treatments
DMSO
MTX-216
MTX-211
Pictilisib
Trametinib
MTX-216+ Trametinib
Cell lines
MeWo
WM3918
SKMEL113
c
PC3 loadings
PC4 loadings
678 genes
315 genes
491 genes
414 genes
(–) PC3 loadings
(+) PC3 loadings
(–) PC4 loadings
(+) PC4 loadings
d
Enrichment by GO Biological Processes
mitochondrial ATP synthesis coupled electron transport (GO:0042775)
respiratory electron transport chain (GO:0022904)
mitochondrial electron transport, NADH to ubiquinone (GO:0006120)
mitochondrial respiratory chain complex assembly (GO:0033108)
NADH dehydrogenase complex assembly (GO:0010257)
mitochondrial respiratory chain complex I assembly (GO:0032981)
mitochondrial respiratory chain complex I biogenesis (GO:0097031)
mitochondrial electron transport, cytochrome c to oxygen (GO:0006123)
cellular respiration (GO:0045333)
aerobic respiration (GO:0009060)
DNA metabolic process (GO:0006259)
mitotic cell cycle phase transition (GO:0044772)
DNA repair (GO:0006281)
DNA replication (GO:0006260)
G1/S transition of mitotic cell cycle (GO:0000082)
centromere complex assembly (GO:0034508)
regulation of mitotic cell cycle phase transition (GO:1901990)
cell cycle G1/S phase transition (GO:0044843)
chromatin remodeling at centromere (GO:0031055)
DNA replication-independent nucleosome assembly (GO:0006336)
(–) PC3 terms
(–) PC4 terms
-log10(FDR)
e
GSEA of genes down-regulated by MTX-216 (Hallmark terms)
ADIPOGENESIS
ALLOGRAFT REJECTION
ANDROGEN RESPONSE
ANGIOGENESIS
APICAL JUNCTION
APICAL SURFACE
APOPTOSIS
BILE ACID METABOLISM
CHOLESTEROL HOMEOSTASIS
COAGULATION
COMPLEMENT
DNA REPAIR
E2F TARGETS
EPITHELIAL MESENCHYMAL TRANSITION
ESTROGEN RESPONSE EARLY
ESTROGEN RESPONSE LATE
FATTY ACID METABOLISM
G2M CHECKPOINT
GLYCOLYSIS
HEDGEHOG SIGNALING
HEME METABOLISM
HYPOXIA
IL2 STAT5 SIGNALING
IL6 JAK STAT3 SIGNALING
INFLAMMATORY RESPONSE
INTERFERON ALPHA RESPONSE
INTERFERON GAMMA RESPONSE
KRAS SIGNALING DN
KRAS SIGNALING UP
MITOTIC SPINDLE
MTORC1 SIGNALING
MYC TARGETS V1
MYC TARGETS V2
MYOGENESIS
NOTCH SIGNALING
OXIDATIVE PHOSPHORYLATION
P53 PATHWAY
PANCREAS BETA CELLS
PEROXISOME
PI3K AKT MTOR SIGNALING
PROTEIN SECRETION
REACTIVE OXYGEN SPECIES PATHWAY
SPERMATOGENESIS
TGF BETA SIGNALING
TNFA SIGNALING VIA NFKB
UNFOLDED PROTEIN RESPONSE
UV RESPONSE DN
UV RESPONSE UP
WNT BETA CATENIN SIGNALING
XENOBIOTIC METABOLISM
FDR = 0.05
MeWo
WM3918
SKMEL113
-log10(FDR)
f
NDUFA1
NDUFB1
UQCRQ
COX5A
P = 4.9×10-6
P = 1.3×10-5
P = 1.6×10-4
P = 1.3×10-8
Normalized transcript (TPM) level
DMSO
MTX-216
Trametinib
MeWo
WM3918
SKMEL113

Figure 6

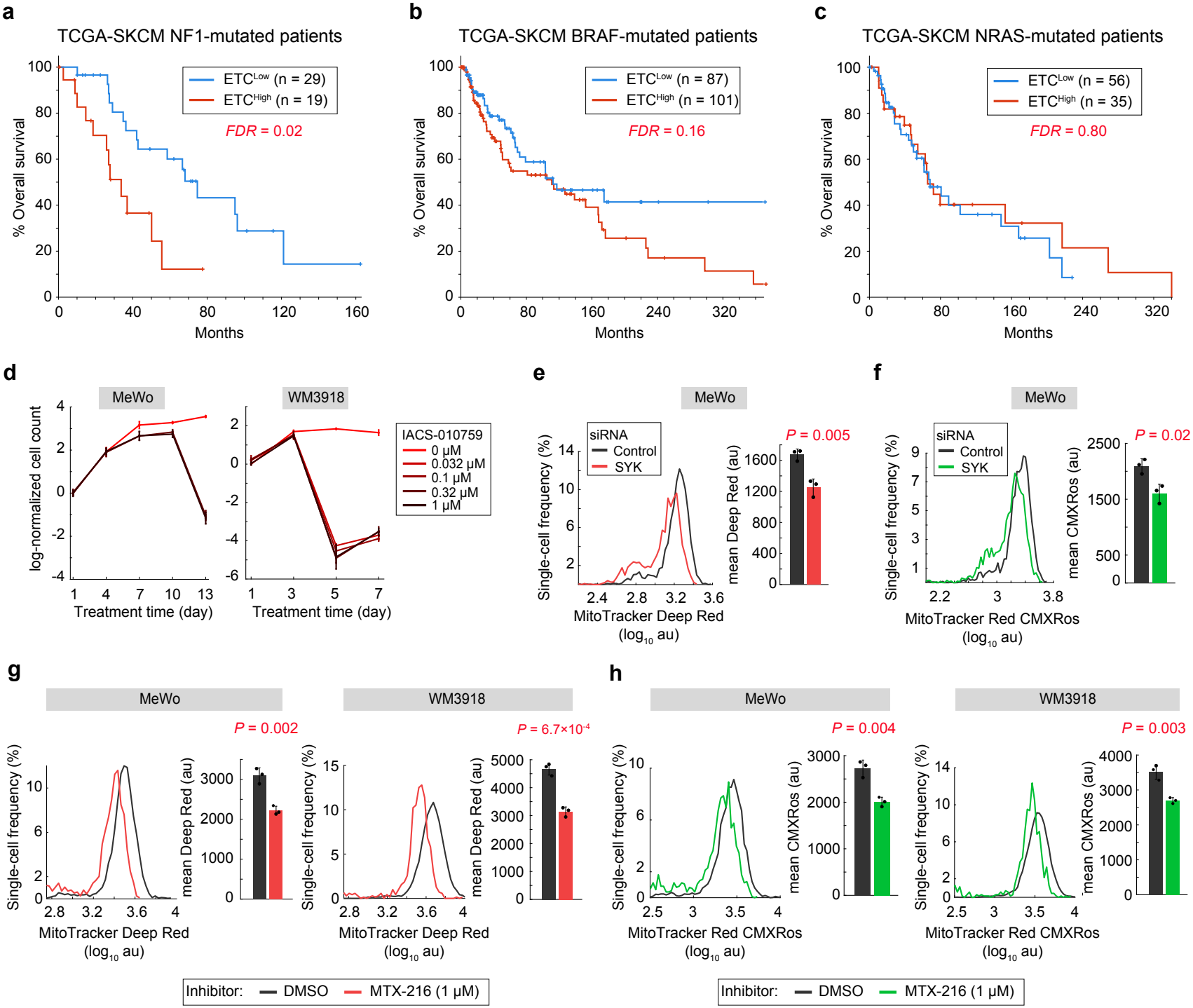
a
TCGA-SKCM NF1-mutated patients
ETCLow (n = 29)
ETCHigh (n = 19)
FDR = 0.02
% Overall survival
Months
b
TCGA-SKCM BRAF-mutated patients
ETCLow (n = 87)
ETCHigh (n = 101)
FDR = 0.16
c
TCGA-SKCM NRAS-mutated patients
ETCLow (n = 56)
ETCHigh (n = 35)
FDR = 0.80
d
MeWo
WM3918
log-normalized cell count
Treatment time (day)
IACS-010759
0 μM
0.032 μM
0.1 μM
0.32 μM
1 μM
e
MeWo
siRNA
Control
SYK
Single-cell frequency (%)
MitoTracker Deep Red
(log10 au)
mean Deep Red (au)
P = 0.005
f
MeWo
siRNA
Control
SYK
Single-cell frequency (%)
MitoTracker Red CMXRos
(log10 au)
mean CMXRos (au)
P = 0.02
g
MeWo
WM3918
P = 0.002
P = 6.7×10-4
Single-cell frequency (%)
MitoTracker Deep Red
(log10 au)
mean Deep Red (au)
Inhibitor:
DMSO
MTX-216 (1 μM)
h
MeWo
WM3918
P = 0.004
P = 0.003
Single-cell frequency (%)
MitoTracker Red CMXRos
(log10 au)
mean CMXRos (au)
Inhibitor:
DMSO
MTX-216 (1 μM)